NUMERICAL SIMULATION OF DETAILED FLOW THROUGH FORMING FABRIC

by

ZHISHUO WANG

B. A. Sc., Tsinghua University, Beijing, P.R.China, 2002

A THESIS SUBMITTED IN PARTIAL FULFILLMENT OF
THE REQUIREMENTS FOR THE DEGREE OF

MASTER OF APPLIED SCIENCE

in

THE FACULTY OF GRADUATE STUDIES

(Mechanical Engineering)

THE UNIVERSITY OF BRITISH COLUMBIA

May 2006

© Zhishuo Wang, 2006

Abstract

The relation between the filament displacement of forming fabric and the wire mark characteristic of final paper product is investigated for the first time. The ultimate goal of this research is to understand the detailed dewatering mechanism of forming section in 3D level as well as provide a guide of forming fabric design and maintenance to obtain paper product with best quality.

A 3D computational model of a square weave single-layer forming fabric has been developed by geometry modeling and commercial CFD software to simulate the detailed dewatering process of forming section. The reliability of the geometric model, grid convergence, solver settings, and boundary conditions are checked. Experimental data of wind tunnel screen is used to indirectly validate this model since currently there is no 3D experimental data of forming fabric available. Accuracy analysis is conduct with GCI (grid convergence index) method, which is widely accepted for CFD error estimation.

Next, the effect of filament's displacement on the upstream velocity distribution, which represents the fiber distribution in the formed fiber mat, is revealed. From wire mark theory, this distribution pattern can directly affect the grammage and wire mark level on paper sheet. The 2D/3D velocity plots of geometric structure with filament displacement are compared with those of uniform structure. Pressure drop and mass flow rate under both cases are also discussed.

The CFD result shows the displacement of forming fabric filaments has a significant adverse influence on the uniformity of the upstream velocity distribution and mass flow rate through different open areas of the fabric. Good agreement between the simulation outcomes and experimental pressure drop values through wind tunnel screens is achieved.

The pressure drop through fabric is independent of the displacement. Therefore, it cannot be used to judge the fabric uniformity.

This numerical model can significantly contribute to the understanding of forming fabric with a low cost. However, 3D experimental work should be done in future to validate this model. More complex CFD models such as multi-phase model also should be developed as the next step to obtain more accurate results.

Contents

Abstract ii

Table of contents iv

List of tables vi

List of figures ix

Acknowledgments x

1 Introduction 1

1.1 Paper making procedure 2

1.2 Forming process 3

1.2.1 Forming in history 4

1.2.2 Fourdrinier Forming 4

1.2.3 Twin wire forming 6

1.3 Forming fabric 8

2 Literature Review 12

2.1 Formation and wire mark 12

2.1.1 Formation 13

2.1.2 Wire mark 14

2.2 Researches on formation and wire mark 17

2.2.1 Experimental researches 17

2.2.2 Numerical researches 18

2.2.3 Industry methods 22

2.3 Conclusion and objective 23

2.4 Approach and assumptions 24

2.4.1 Approach 24

2.4.2 Assumptions 25

3 Modeling and Validation **27**
3.1 Modeling 28
3.1.1 Geometry modeling 28
3.1.2 Grid generation and grid convergence 32
3.1.2.1 Grid generation 33
3.1.2.2 Grid convergence 34
3.1.3 Geometric model validation 35
3.1.4 Solver selection and settings 37
3.1.4.1 Solver selection 37
3.1.4.2 Steady and unsteady 39
3.1.4.3 Boundary conditions 41
3.2 Iteration convergence judgment 43
3.3 Accuracy analysis 45
3.4 Wind tunnel screen validation 46

4 Results and discussion **51**
4.1 Velocity distribution 51
4.1.1 Data acquisition 52
4.1.2 Plane velocity results 53
4.1.3 Rake velocity results 63
4.2 Mass flow rate 67
4.2.1 Data acquisition 69
4.2.2 Mass flow rate results 70
4.3 Pressure drop 71

5 Summary and Conclusions **73**
5.1 Summary 73
5.2 Conclusions 74

6 Suggestions for future work **75**

Appendix A Grid Convergence Independence(GCI) procedure **77**

Appendix B Mass flow rate validation **79**

List of Tables

3.1 Pressure drop values and point velocities of five different grid sizes. 35
3.2 Mass flow fluxes of inlet and outlet and the net mass flow flux. . . 44
3.3 Geometry dimensions of tested forming fabric and NACA wind tunnel screens. 46

4.1 Mass flow rate difference between normal pore and enlarged pore of forming fabric. 70

List of Figures

1.1 A schematic drawing of one modern Fourdrinier machine. 5
1.2 A picture of one modern Fourdrinier machine. 5
1.3 A picture of twin wire forming machine. 6
1.4 A close-up scheme of twin wire former. 7
1.5 The examples of single-layer, double-layer and triple-layer forming fabric [1]. 9

2.1 Laboratory sheet with the marks generate from a double-layer forming fabric [1]. 14
2.2 Wire mark mechanism and its influence on printing [2]. 15
2.3 The geometric structure of a commercial triple-layer forming fabric in Zhaolin's research [3]. 20

3.1 An isometric view of the calculation domain for the uniform fabric. 29
3.2 Top view and front view of the geometric structure of the uniform fabric. 30
3.3 An example of the fabric geometric model with filament displacement. One CMD filament has a displacement of 25% filament spacing in positive MD. 31
3.4 An example of multi-filaments move together. The right three CMD filaments are moved toward positive MD with a displacement of 20% normal spacing. 32
3.5 Hybrid computational mesh scheme applied in this research. . . . 33
3.6 Pressure drop results of the case with 5% spacing displacement, under seven different grid sizes. 34
3.7 Pressure distributions along the Z-direction of the forming fabric of four different grid sizes. 35
3.8 Velocity vector plot of the calculation domain. 36
3.9 Fluctuation of static pressure on certain point in unsteady case. . 40
3.10 The variation history of static pressure on certain point in steady case. 41

3.11 Comparison of velocity profiles from steady and unsteady model. . 42
3.12 The boundary conditions of the domain. 42
3.13 A typical residuals plot of a steady case. 44
3.14 The variation history of velocity magnitude of certain spot in the flow field during iteration. 44
3.15 Pressure-drop coefficients for flow incident at angle θ and freely deflected by screen. All curves are drawn for θ=0° [4]. 48
3.16 Comparison of CFD and experimental results of pressure-drop coefficient K as a function of local Reynolds number. 49

4.1 Location of the sectional plane (Plane 1) used in data acquisition for 3D velocity plots. 52
4.2 Locations of Rake 1 and Rake 2 using in data acquisition for 2D velocity plots. 53
4.3 Isometric view and top view of the velocity magnitude contour at Plane 1, uniform mesh case, real space coordinate system. 54
4.4 Isometric view of the velocity magnitude contour at Plane 1, uniform mesh case, Z-axis is the velocity magnitude in Plane 1. . . . 55
4.5 Isometric view and top view of the velocity magnitude contour at Plane 1, with 30% displaced filament, real space coordinate system. 56
4.6 Isometric view of the velocity magnitude contour at Plane 1, with 30% displaced filament, Z-axis is the velocity magnitude in Plane 1. 57
4.7 Isometric view and top view of the MD velocity component contour at Plane 1, uniform mesh case, real space coordinate system. . . . 59
4.8 MD/CMD velocity vectors in Plane 1, uniform mesh case. 60
4.9 Isometric view of the MD velocity component contour at Plane 1, uniform mesh case, Z-axis is the MD velocity in Plane 1. 60
4.10 Isometric view and top view of the MD velocity component contour at Plane 1, with 30% displaced filament, real space coordinate system. 61
4.11 MD/CMD velocity vectors in Plane 1, with 30% displaced filament. 62
4.12 Isometric view of the MD velocity component contour at Plane 1, with 30% displaced filament, Z-axis is the MD velocity in Plane 1. 62
4.13 Velocity magnitude profiles along Rake 1 with different filament displacements. 63
4.14 MD velocity profiles along Rake 1 with different filament displacements. 64
4.15 Velocity magnitude profiles along Rake 2 with different filament displacements. 65

4.16 MD velocity profiles along Rake 2 with different filament displacements. 65
4.17 Effect of displacement of multiple filaments on velocity magnitude along Rake 1. 66
4.18 Effect of displacement of multiple filaments on MD velocity component along Rake 1. 67
4.19 Effect of displacement of multiple filaments on velocity magnitude along Rake 2. 68
4.20 Effect of displacement of multiple filaments on MD velocity component along Rake 2. 68
4.21 Isometric views showing the location of Plane 2 and Plane 3. . . . 69
4.22 Difference between mass flow rate through enlarged area and through uniform areas, as a function of filament displacement. 71
4.23 Pressure drop versus Z-position through forming fabric. 71
4.24 Pressure drop through forming fabric as a function of filament displacement. 72

6.1 A typical 2/5 shed triple layer forming fabric(without binding yards). 76
6.2 The geometric structure of the forming fabric with filament displacement. 80
6.3 Normalized mass flow rates under difference normalized offsets. . . 81

Acknowledgments

First and foremost, I would like to express my deepest gratitude to my research supervisor Dr. Sheldon I. Green for his patient guidance, continuous inspiration and endless support.

Secondly, my appreciation is due to Dr. Carl Ollivier-Gooch and Dr. James Olson for participating on my research committee, and for their help and guidance.

Many other professors include Dr. R.J. Kerekes, Dr. W.K. Bushe, and Dr. Calisal also gave me very useful horizons and suggestions. I will also show my respects to them.

I would like to thank all the people who helped me during my study and research period. The technician of Pulp and paper center, Tim Paterson, always be ready for help me about the computer utilities. Alan Steeves, Jay Zhao and Perry Yabuno from Department of Mechanical Engineering provided me the computer network support and engineering software. I also owe a great deal to my colleagues at UBC specially Zhaolin Huang, Tim Waung, Seth Gilchrist, Larry Li, Satya Mokamati, Ali Vakil and Roozbeh. I cannot expect a better research team.

I also wish to express my sincere thanks to Dr. Sheldon I. Green, Asten Johnson and NSERC for their financial support.

Last but not least, I am forever indebted to my parents for their unselfish support and encouragement.

Chapter 1

Introduction

Paper is one of the most significant inventions of human being throughout the history. It has been serving as a major intermediate of our society from the beginning of its birth. Nowadays, a big variety of paper products have been made and used on various purposes. Paper consumption all over the world has been over three hundred million tons per year [5] and is still increasing. A large part in this statistics is printing paper, which is required to have a smooth and uniform surface. Determining how to make paper with high surface quality is a very practical concern and is the motivation of this research.

In microscopic sense, paper is a heterogeneous three-dimensional composition dewatered from a water-fiber suspension with non-fibrous additives, which is known as pulp. This dewatering process basically occurs in the forming section of papermaking machine and it has been observed that the structure of the final paper sheet has already been fixed after this forming process. So try to understand the microstructure characteristics of pulp and formed fiber sheet during the forming process is a correct direction.

Forming fabric is a key component in forming section. The fiber suspension is dewatered on it to form the raw paper sheet. It is believed that the topography of forming fabric has a fundamental interaction with the sedimentation characteristic of fiber suspension. This characteristic has a direct influence on the structure of fiber sheet hence the surface quality of commercial paper product. Based on above analysis, the relation between forming fabric surface topography and fiber suspension movement became a major topic. The ability to optimize

forming fabric design has been shown to give the papermaker added value both in terms of increased productivity and improved quality.

In this chapter, firstly a brief introduction of papermaking process is presented, and then followed by the detailed description of the forming section of papermaking machine. In the end, some related concepts of forming fabric are further discussed. This background section is to eliminate the reading obstacle.

1.1 Paper making procedure

It is believed that the art of true paper making had its origin in 105 A.D. in China. [1] Tsai, Lun initiatively made out the first practical and relatively economical procedure of papermaking. In his method, paper was originally produced from fermented and beaten mulberry bark fibers. The fibers were suspended in water and scooped out with a screen made of bamboo splinters. This method was kept secret from the rest of world for several hundred years until the Arab army's invasion. Arabs learned the art from captured Chinese papermakers and spread to all Arab domains then passed into Europe with wars. Papermaking finally came to the North American continent in 1690 with the setting up of a papermaking mill built by William Rittenhouse and William Bradford in Pennsylvania.

After centuries, papermaking has evolved to a modern interdisciplinary industry with many high technologies. The complex procedure of papermaking involves four basic stages: pulp manufacturing, stock preparation, paper sheet forming and paper sheet finishing. The first step is usually done in pulp plant whereas the other three stages are carried out on the production line of a huge, comprehensive, and highly automatic paper machine in paper plant.

Today, wood is the primary raw material from which large majority of paper pulp is made. So the procedure begins in the woodlands where trees are cut into prescribed lengths. Then the barks are all removed and logs are reduced to chip form approximately one-half to three-quarters of an inch in size. These chips are conveyed to vibrating screens where oversized chips are eliminated. Wood chips are discom-

posed into cellulose fibers and other undesirable components by one or more of the three prevalent pulping methods: mechanical pulping, chemical pulping and semi-chemical pulping. Bleaching is applied at the end of pulping stage.

After pulp treatment, fillers, dyes and additives are blended into pulp to enhance specific characteristics of paper. Refining is also done to increase the capacity of water absorbing and improve sheet formation as well. Variety types of blended pulp are mixed and pumped into the headbox then be uniformly sprayed onto the forming fabric in forming section from headbox slice. Water in fiber suspension is removed by its weight on the forming fabric and the formed fiber sheet is carried by the cycled forming fabric to pressing section and drying section in turn. Further dewatering process forced by high pressure/vacuum or high temperature, respectively. The consistency of fiber suspension changes from 0.1%-1% in the headbox to over 95% after passing above three dewatering sections.

The dried sheet then comes into the finishing stage of the procedure. The major process in finishing stage is calendering, which irons the paper sheet between heavy polished steel rollers to acquire a much smoother surface. Final treatments including trimming, slitting, and converting are necessary to get customer paper products, such as printing paper, envelopes, grocery bags, paper cups, etc. Comprehensive quality control, including raw material test, pulp test and final product test [6] is applied during the whole papermaking procedure.

Since the forming fabric topography and pulp movement in forming process is the concerns of this study, only forming section and forming fabric are detailedly informed in next sections.

1.2 Forming process

The forming or dewatering process, basically in forming section, has the most significant impact on the surface quality of final paper sheet. Major forming methods along history are introduced in this section.

1.2.1 Forming in history

Filtering pulp through a fine mesh screen can form a fiber mat which was tested suitable for writing. Based on this fact, a handcrafted dewatering method, floating mold forming was applied by Tsai, Lun in ancient China. [7] Floating mold was a wooden frame with a stretched woven-crossing cloth filaments screen. Fiber suspension with certain consistency was poured onto the mold submerged in water. Water was drained through the cloth screen with the upward movement of the mold and as a result, a fiber web was formed on it. After being thoroughly dried, the fiber sheet can be detached from the screen and that finishes the procedure. This cloth screen is the precursor of the forming fabric, which played a crucial role in the papermaking craft.

While there was only little change in forming principle, many high-efficiency advances which reformed the forming procedure of papermaking from a manual craft to a modern industry had been involved during the industry revolution. At the end of 18th century, papermaking got an important progress that the continuous moving fabric belt was introduced by Nicolas Louis Robert (1761-1828). [8] His invention made it possible to get endless paper sheet continuously, take place of the historical batch or semi-batch way. At the same time, it also overcame the dimensional and output limitations of paper product by old methods. Nicolas' application is the prototype of modern paper machines, and the dimension and working speed keep increasing ever since it.

1.2.2 Fourdrinier Forming

The first high speed paper machine was successfully built and tested by Fourdrinier brothers in British in 1807 after their multi-years' endeavor. The machine was named by its inventors and known as Fourdrinier machine nowadays. Function enhancement of the machine always happens during these two centuries. A schematic drawing of one modern Fourdrinier machine is shown in Figure 1.1. Its picture is shown in Figure 1.2.

The key part of the Fourdrinier machine is a continuous wire mesh belt that moves horizontally, which is known as forming fabric. This design

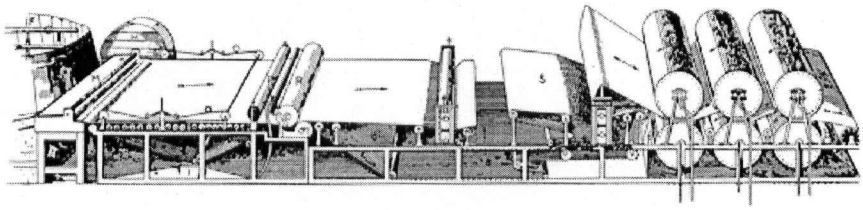

Figure 1.1: A schematic drawing of one modern Fourdrinier machine.

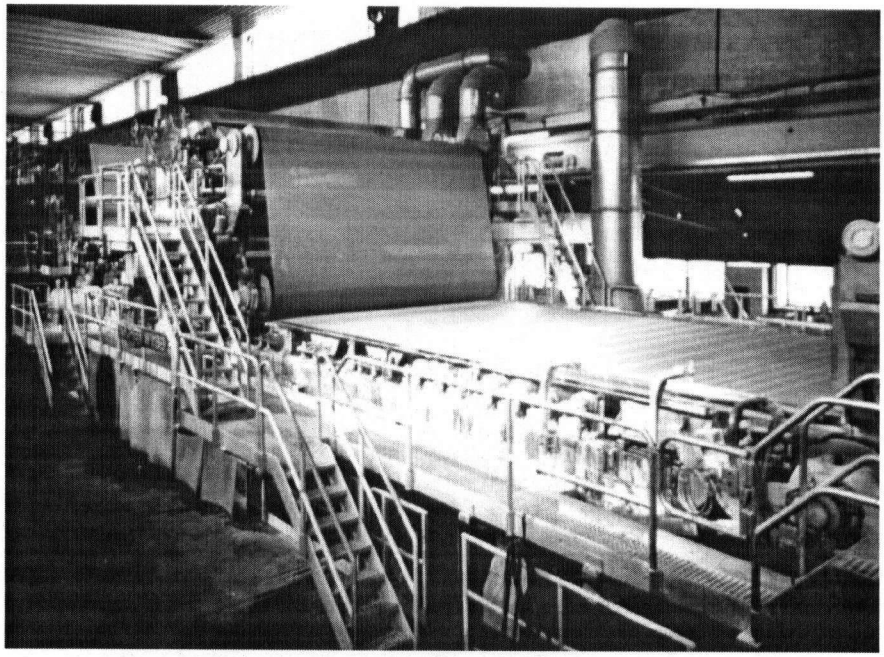

Figure 1.2: A picture of one modern Fourdrinier machine.

makes it's possible to conduct continuous and automatic production. A flow of watery pulp injected from headbox slice spread on the fabric and passes over a number of rolls. A shallow wooden box beneath the fabric catches much of the water that drained off during this stage. This water will be remixed with the pulp to salvage the fiber contained in it. Spreading of the fiber sheet on the forming fabric is limited by rubber deckle straps moving at the sides of the fabric. Suction pumps beneath fabric hasten the drying of the paper, and fabric itself is moved from side to side to aid the felting of the fibers. Forming fabric and drained fiber mat will get separate at the end of the forming board. The former will be cleaned along the way of back to the vicinity of headbox slice. The latter will be transferred to the press section to get further drainage. A dandy roll on the forming board is for impress the watermarks that identify the grade of paper and the maker.

1.2.3 Twin wire forming

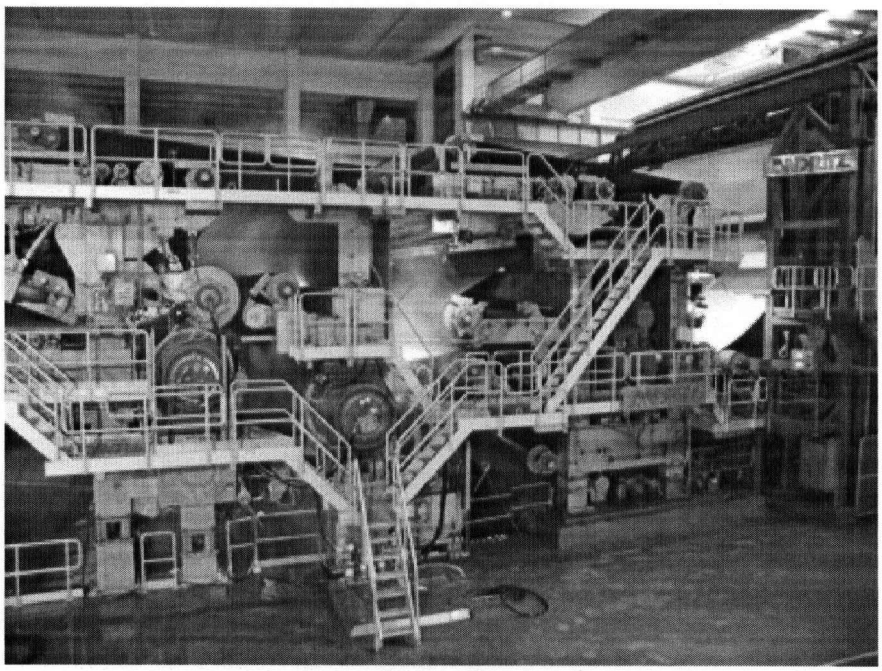

Figure 1.3: A picture of twin wire forming machine.

The first modern twin wire former, or 'gap former', was invented by David Webster in 1953. It was developed to not only avoid the heavy pulp splashing under high speed operation condition, but also eliminate the dual-sidedness problem (visual differences between paper's

two sides) associated with single wire Fourdrinier machine. The operation speed of a typical twin wire machine is around 2000 m/min [1], doubles the maximum acceptable speed of Fourdrinier machine. Figure 1.3 shows a picture of twin wire forming machine.

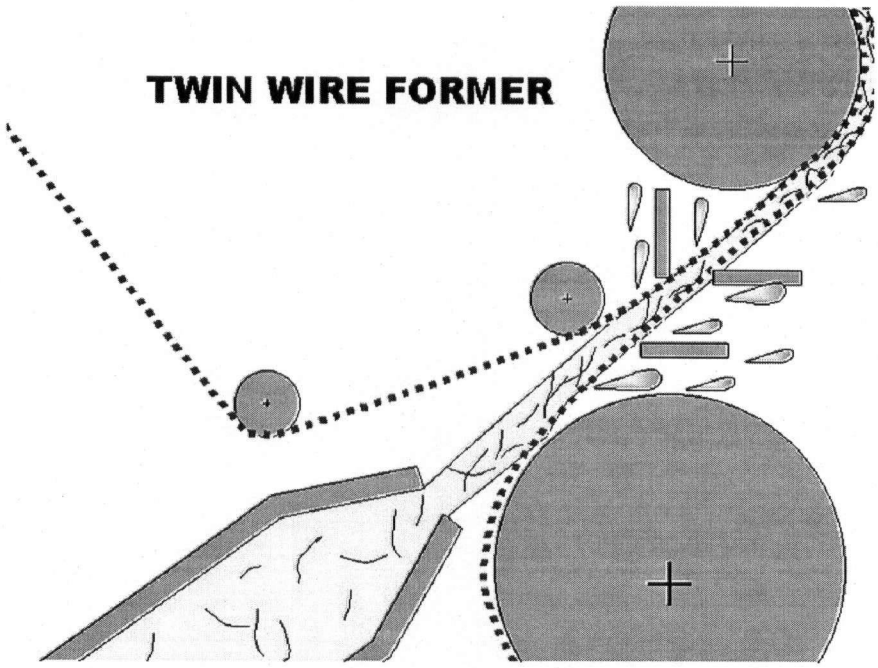

Figure 1.4: A close-up scheme of twin wire former.

Figure 1.4 shows a close-up scheme of a twin wire former. In twin wire forming machine, the pulp jet from the headbox is directed into the narrow gap between two forming fabrics (twin wires). Water is removed in both wire surfaces. This bi-directional drainage mechanism tends to form a sheet which the appearances of the two sheet sides are identical and gain excellent product consistency. The rate of dewatering process is enhanced by passing the pair of forming fabrics along fixed obstacles, such as suction boxes and blades in blade shoe, and rotating cylinders, such as rolls. The high pressure gradient crossing the forming fabric in the vicinity of those components can dramatically improve the dewatering capability. In this case the wires are sheets of Polytetrafluoro ethylene (PTFE) mesh designed for the ease of water drainage.

After the application of twin wire former, other types of paper machine have also been developed, such as hybrid-former and multi-fabric for-

mer. There is no innovation on the basic forming mechanism. They are mere a combination of Fourdrinier/twin wire machine and multi Fourdrinier machines, respectively. Hybrid-former can afford the maximum dewatering rate, while multi-fabric former is specific designed for making multi-layer paper product such as paper board.

1.3 Forming fabric

In forming section, forming fabric acts as a filtration media through which water is drained out of the fiber suspension. At the same time, it also serves as a pulp transport tool and smooth support base from headbox to press section. The working speed of it vary from 100 m/min up to approximately 2000 m/min. Forming fabric is a fine cloth mesh woven by polyester and polyamide filaments, and seamed to an endless loop to satisfy the requirement of industry's continuous operation. The individual filament of forming fabric is curvy thread, which has a circular cross-section with a few tenths of millimeters in diameter. The spacing between filaments is usually around 2 to 3 times of the filaments diameter. These sizes afford light wear mark as well as possibility of water removal.

There is a variety of forming fabric in application, with the most common structures being single-layer, double-layer, double-layer extra weft added, triple-layer, and triple weft. All of them have a weaving structure composed by filaments oriented in two orthogonal directions of the fabric plane, machine direction (MD) and cross-machine direction (CMD). Different forming fabrics have different number of layers in their vertical cross-section. Figure 1.5 shows the examples of single-layer, double-layer and triple-layer forming fabric. Single-layer fabric is made of one CMD filament layer. Double-layer fabric has two CMD filament layers. Triple-layer fabric is actually consists of two single-layer fabrics bound together by a layer of binding filaments. The construction of a forming fabric is complex and three-dimensional. Beside the weaving structures in MD and CMD, the filaments are also woven together by weft in the vertical Z-direction.

With an exception of single-layer fabric, forming fabrics have two distinct surfaces, forming surface(paper side) and wearing surface(machine

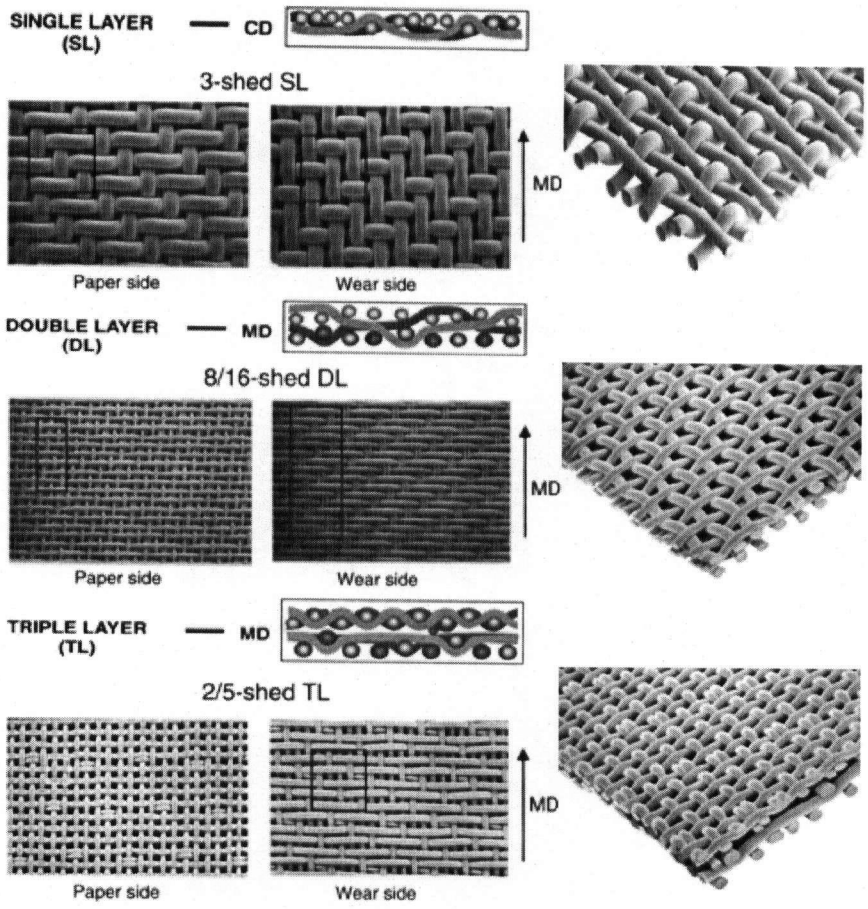

Figure 1.5: The examples of single-layer, double-layer and triple-layer forming fabric [1].

side). To get a high retention(fiber retainment) effect, paper side surface should have very fine filaments and small pore size. On the other hand, to have a good wear- resistance, wear side surface should be as coarse as possible. Multi-layer fabrics give the best solution of this requirement. They can have two surfaces with very different filament and pore sizes.

The shed count of a fabric is determined by the number of MD/CMD filaments after which the weave pattern repeats identically. For example, considering a 3-shed single-layer fabric as shown in Figure 1.5, the weave pattern is repeated after every three MD/CMD filaments. In double or multi-layer fabrics, paper side could have a different shed count with the wear side. Still refer to Figure 1.5, if the paper side of a double-layer fabric is 8-shed and the wear side is 16-shed, the shed count of this fabric will be marked as 8/16-shed. In triple-layer and triple-weft fabrics, it is normal to use different shed counts on paper side and wear side.

Important properties of forming fabric include drainage/retention capability, sheet supporting, mechanical stability, wear resistance, and marking level. With the help of dewatering elements, forming fabrics typically have high dewatering capability to fit operation speed of paper machine. However, depending on the paper grade requirements, slow drainage may be desired. Fabric's drainage properties must match to achieved paper grade. Sheet supporting is an ability to retain fibers for achieving strong paper sheet to pass through press section, and retain fines for good opacity. Mechanical stability refers to its ability to run for long term without excessive stretching or wrinkling. Wear resistance is an anti-abrade property related to fabric's life time. Marking level is a benchmark for the mark level of achieved paper sheet.

In paper making industry, forming fabric is selected by its runnability features and achieved paper quality features. Runnability features basically include cleanliness, dewatering feature, guidance, and wear stability. Different types of former have different runnability requirements. For example, in twin wire formers, DL-HWD type fabrics are most common because of their good diagonal stability and low water carrying ability. Product quality features refer to the achieved paper's

property of absorption, formation, strength, moisture, marking level, porosity, etc. Wire mark level is the only concern of this study. (Please refer other literature [8, 6] for further information of other properties.) Practically, paper grade is used as an assessment system of product quality. Single-layer fabrics are often selected for making packaging papers/boards, WF fine paper or tissue. As for newsprint or mechanical printing papers, triple-layer or triple weft fabrics are widely applied.

In this chapter, background knowledge of this research has been provided. Next, literature review of related domain will be summarized. Then the scope and approach of this study will be discussed.

Chapter 2

Literature Review

In previous chapter, related background knowledge of papermaking industry has been introduced, and physical properties and functions of forming fabric have been clarified. The concern of this study is the interaction between the forming fabric structure and sheet wire mark level. This chapter contains a literature review of this topic. From current research outcomes, it is clear that the correct application of forming fabric is a key point to gain paper product with high surface quality, more specifically, shallow wire mark.

There are numerous documents (e.g. [9, 10, 11, 12, 13, 14]) that focus on other forming fabric properties such as permeability, retention, runnability, etc. Although these topics are also very important, they won't be involved in this thesis to avoid distractions.

2.1 Formation and wire mark

Formation is most commonly defined as the density difference of paper sheet when looking it through. It generally used to describe macro-scaled areas of varying density which can be easily seen by human eyes [2]. Wire marks are small impressions produced on the bottom surface of paper sheet [8]. It is used to explain the micro-scaled density variation which is caused by the structure of the forming fabric on which the fiber mat is formed. Both of them are very important surface properties that influence the paper general appearance. From a utility view point, they affect sheet print properties such as ink penetration and absorbency [6, 15]. No matter in which way the density variations come from, by large scale flocs or fine scale wire mark, the

gloss appearance of final printing quality is identical.

2.1.1 Formation

An ideal formation is a sheet which has completely uniform macro-density distribution. Sheets with areas of varying density are said to be flocky or cloudy, which is obviously an adverse factor of printing quality. In paper forming process, pulp uniformity, mobility and fiber's superposition are three major factors of the fiber suspension which determine the quality of formation [16]. Here mobility refers to the freedom level with which fibers can move relative to one another.

Dilution is the principal method for increasing fiber suspension uniformity and mobility [17]. For this reason, the pulp consistency in headbox is generally controlled in the range of 0.5% to 1%. Smith [18] has shown that under smooth drainage conditions, formation first worsened, then improved, and worsened again with the consistency increase. He hypothesized that this varying pattern come form changing regimes of inter-fiber contact in the suspension. Another remarkable and interesting fact is from E.S. Brazington's research [19]. He found nonuniform pulp may lead to good mat formation too. It is because fiber redistribution can readily be achieved by hydrodynamic forces during the drainage process. Consistence does not determine the formation quality alone. It has been quantitatively shown by Jokinen and Ebeling [20] that fiber length also has a sizable effect on paper formation. The third factor is superposition. The piling up of fibers and flocs upon one another in themselves imposes a level of web uniformity, different from that in the suspension. For example, Gorres et al. have shown that superposition of flocs of low density leads to improved formation in fiber mat [21].

Headbox design and performance have the largest major effect on sheet's macro scale formation. High machine-directional fiber orientation has already existed in the headbox before the injection. This, together with the turbulence created by stationary elements on forming board, largely dictates the macro scale formation of final paper sheet.

Forming fabric can affect sheet's macro scale formation in two different ways. On one hand, the design of fabric determines the drainage rate of the initial and subsequent fiber mats, which slightly affects the formation. On the other hand, its surface topography can left some marks in large scale on the initial fiber mat. Danby's experimental research [2] shows that the initial fiber mat formed on a fabric is very greatly influenced by the surface structure of the filtering medium on which it settles. A fine, uniform support grid will give a more uniform initial fiber mat than a coarse, non-uniform one. This degree of initial uniformity in fact influences subsequent layers of fiber as the sheet is formed.

2.1.2 Wire mark

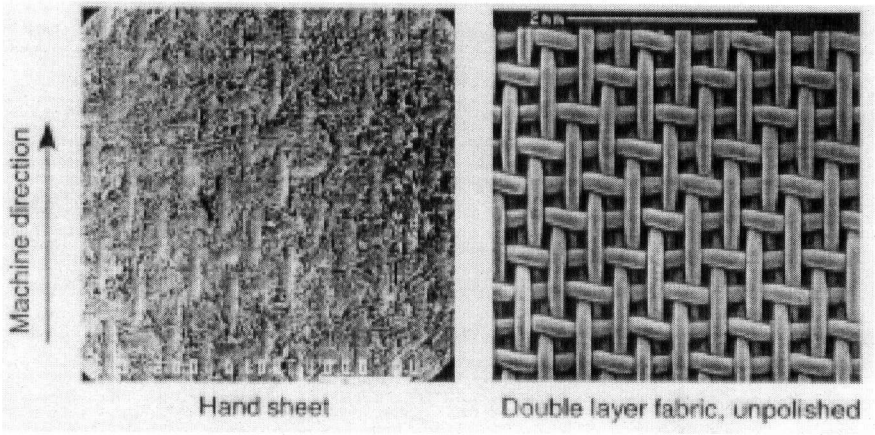

Figure 2.1: Laboratory sheet with the marks generate from a double-layer forming fabric [1].

Wire mark is used to explain the micro or finer levels of density difference which are caused by the structure of the forming media on which the sheet was produced. Visible wire marking can be considered as a combination of topographical marking and drainage marking. Topographical marking is an image of the top surface of a forming fabric in the sheet of paper caused by fibers following the water flow out of the sheet emphasized by suction, or compression of the sheet against the fabric. Drainage marking means unevenly distributed fines and fillers in x-y-plane of the sheet according to the drainage channels of a forming fabric.

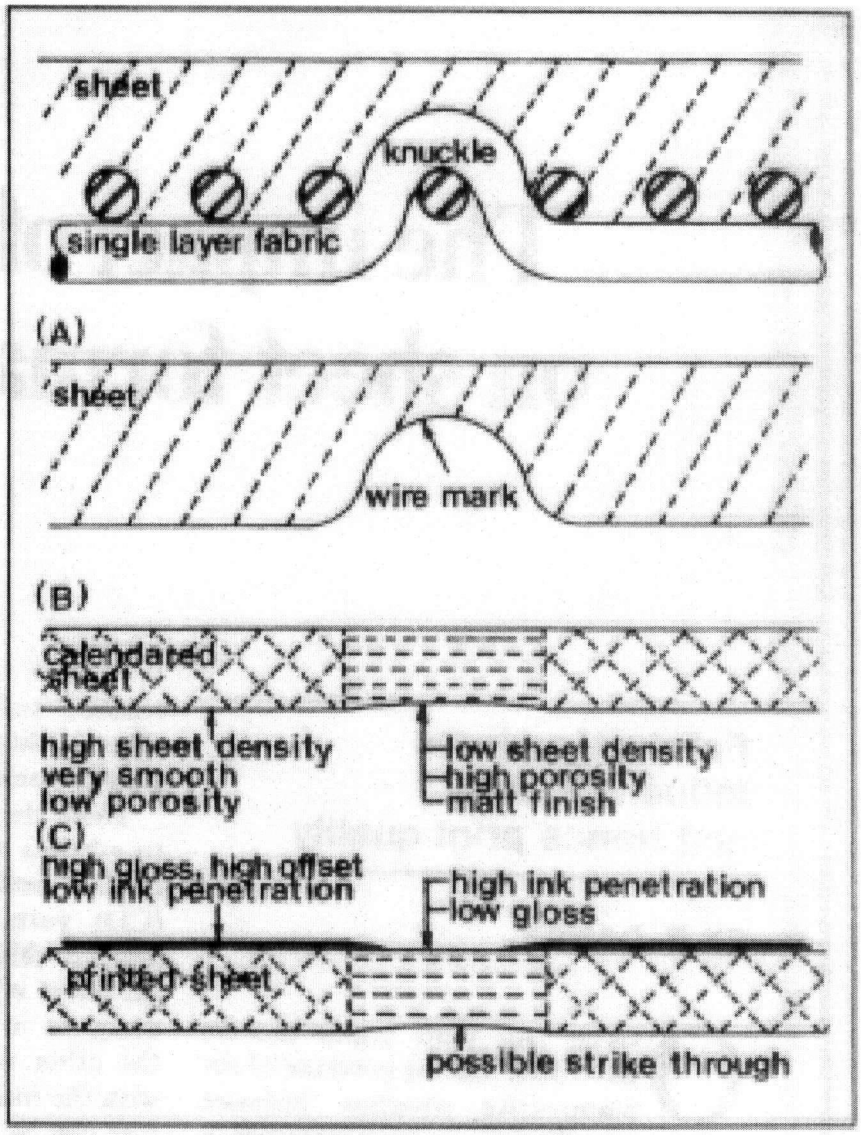

Figure 2.2: Wire mark mechanism and its influence on printing [2].

Figure 2.1 is the picture of a laboratory sheet that shows the marks generate from a double-layer forming fabric. The effect of the wire mark on the sheet surface is clear. The light and dense areas are those formed over the knuckles of the forming media. Between the fabric knuckles, the sheet has partly penetrated into the fabric. Formed over those open areas, the sheet is heavy-colored and porous in fines. After the forming section in paper machine, the sheet will be made flat in wet pressing and further stages. However, the nonuniform density distribution of the fiber mat still keeps some wire marks on the final product.

Figure 2.2 illustrates the way in which wire mark is caused and its influence on printing:

(A) When a sheet is being formed on forming medium it will be made up of thick areas over the pores and thin areas over the knuckles.

(B) During pressing and calendering the thick areas are compressed more than the thin areas, which results in a sheet having differences in density.

(C) The paper properties of the resulting sheet will therefore be high gloss, very smooth and with low porosity in the areas of high density while low gloss, rougher and with higher porosity in the areas of low density.

The high density areas, when printed, will have low ink penetration which will result in high gloss. On the other hand, the areas with low density, or the sheet over the knuckles will have greater ink penetration. With the high porosity, print strike through may occur to the opposite side of the sheet.

Wire mark cannot disappear after further treatment. For example, strong topographic marking still will show up in supercalendered sheet or even coated paper grades. For paper grades that are sensitive to wire marking, a forming fabric with the top side surface made of as small filaments as possible needs to be chosen to reduce the uneven distribution of fibers. The filaments need to be distributed uniformly as well. Any diagonal or cross-machine direction lines in the structure can easily cause drainage marking in initial formed fiber layer. This kind of wire mark could even cause the non-uniformity in large scale formation through the interaction between initial and subsequent fiber layers.

2.2 Researches on formation and wire mark

A lot of experience on forming fabric selection has been gathered from huge amount of engineering practice. Generally speaking, accommodating greater drainage with good fiber retention while minimizing wire mark requires utilizing finer mesh fabrics with smaller diameter filaments in the paper side [22]. Fabric suppliers develop triple-layer fabrics that pair a fine mesh top layer for dewatering with a coarse and durable bottom layer to fulfill mechanical stability requirements and enhance fabric life. However, research institutes are searching something beyond the experience of wire mark control. Although currently forming fabric researchers still cannot come up with a relevant theoretical method to fully characterize the drainage behavior of a forming fabric [1], there are many studies on the relation between wire mark and forming fabric structure. The research outcomes about wire mark can be applied to formation issues.

2.2.1 Experimental researches

During the nearest two decades, R.Danby carried out a series of experiments on wire mark forming theory [2, 15, 23, 24, 25]. Accumulative photographic samples gathered by him provided a clearly intuitive illustration of most his research achievements.

In early researches [2, 23] he compared the effect which the evolution from single-layer through double-layer to triple-layer forming fabrics has had on paper quality, specifically on formation and wire mark. The tools used to conduct the comparison are the eye-strike level of the twill pattern formed by the knuckles of the fabric, the photographic observation, and more standard, the measured NUI (Non-uniformity Index, lower NUI means better uniformity) on production sheets. The conclusion from all these three approaches coincide one another that triple-layer forming fabric has the better sheet structure uniformity and hence better print quality than single-layer, early or later generation double-layer forming fabrics.

Danby also checked the two sides of sheets produced on twin-wire and hybrid (top-wire) formers [23]. Photographic evidences are collected to show that formation and surface characteristics of a sheet produced on

twin-wire and hybrid formers are greatly influenced by the structure of forming fabric pair between which the sheet is formed. The pattern of micro-density differences in the sheet corresponds to the pattern of the forming fabric surface on which each side was formed [25]. The degree of visual two-sidedness, measured by Parker Print Surface(PPS) numbers, can almost equal to the poor two-sidedness level of the sheet made on Fourdrinier machine with single-layer fabric. But by carefully selecting the type of fabric pair, which composed by the convey fabric and the back fabric, the degree of two-sidedness can be almost eliminated. Therefore the advantage of twin-wire and top-wire formers on reducing the two-sidedness can be achieved.

Next, Danby related the impact of forming fabric structures on print quality [15, 23, 25]. The prefect print is one where all ink dots are perfectly round, all are exactly alike, and absorb into the sheet at the same rate. Imperfectly structure uniformity of the sheet surface caused by forming fabric will have an adverse effect on these. He conducted a close examination of the print surface with flocks [15]. The result reveals that the unacceptable print is caused by gloss variation on the surface resulting from variations in ink penetration. These variations stem form the inherent density differences caused by the forming fabric structure. The light areas in the sheet, which correspond the areas above the knuckles of forming fabric, have resulted in unprinted(missing dots) areas in the print.

The relation of fiber lengths and the drainage pore sizes in the forming fabric can also affect the print quality. Same machine type and same fiber lengths with different forming fabric size were producing quite different printing results. Basing on empirical laws, an engineered new generation of intrinsic weft triple-layer fabrics was designed to fit the fiber suspension with certain average fiber length [25].

2.2.2 Numerical researches

Numerical method has been playing more and more important role on forming fabric researches. R.Danby developed an engineering approach to select the optimum forming fabric designs for high-speed papermaking machines [24]. By incorporating the basic principles of

the PAPTAC G18 data sheet into a simple computer program, all forming fabrics can be compared and evaluated. This evaluation provides are approaching in understanding the relation between fiber lengths, forming fabric support at the point of filtration, machine configuration and achieved paper grade/print quality. The parameters in the data sheet related to the print quality are total top surface drainage area, MD/CMD dimensions, Beran Fiber Support Index to name but a few.

Using the Image Analysis techniques devised for measuring density differences of the sheet, D.Chaplin developed a computer program in which these numbers could be used to simulate the absorption rate of printing ink into the sheet, corresponding to the micro-density differences for the printing process [26]. The results correlated well with those obtained on the commercial printing press. But in his assessment system, quality of both the commercial and the computer simulated printed samples was evaluated by human view only, which is open to variations in personal judgment.

Furthermore, H.Zhou and R.Danby introduced a numerical rating for Paper/Print Quality Index, Floc Index and Void Index [27]. This technique can be used to quantify the differences between batches produced at different times on the same machine or to compare the same grade from different sources. Besides, to avoid the misleading information given by conventional methods which use whole sheet formation as an average of the two sides, their program shows that formation when viewed through each of sheet side after splitting. The usage of both split sheets for twin wire formers and whole sheets produced on Fourdriniers is a true representation of the printing potential of the two sides of any one sheet. H.Zhou and R.Danby's research provides a very useful tool to numerically evaluate not only the paper quality including the formation and wire mark level, but also the final print quality that will be achieved on the printing press.

Above numerical applications are about setting up the computer-based intelligent databases to evaluate either the relation between forming fabric data and printing quality or paper surface properties. The computer aid methods of directly modeling the paper sheet and forming

fabric have also come into reality. Paper understanding as a computation of thousands of individual particles assembled together started with the statistical work of Corte and Kallmes [28]. Then, with the increasing capacities of computer, models have extended and become more and more accurate and comprehensive [29].

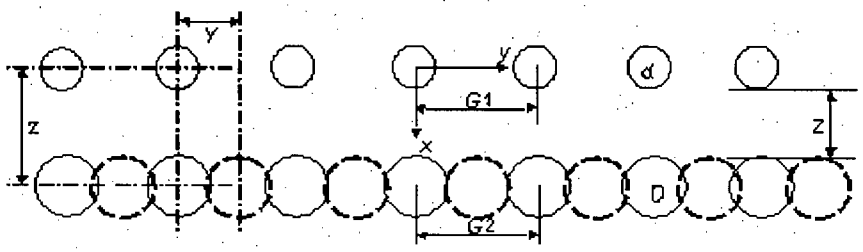

Figure 2.3: The geometric structure of a commercial triple-layer forming fabric in Zhaolin's research [3].

Zhaolin Huang developed a 2D computational model to investigate the details of fiber suspension flow through the forming fabrics [3]. Single-phase, laminar water flow was applied as the media, because of the low consistency of the fiber suspension and low Reynolds number (less than 100) based on filament's diameter. Next, he omitted the cross machine direction (CMD) filaments and simplified the fabric geometry to unequal sized cylinder arrays, which is the projection of machine direction (MD) filaments on the vertical cross-section in Z-direction. The 2D structure of a commercial triple-layer forming fabric in Zhaolin's research is shown in Figure 2.3. The paper side finer MD filaments were reduced to a row of cylinders with small diameter and the machine side coarser MD filaments project a row of bigger cylinders.

Firstly, his CFD schemes were successfully validated by comparing the frequency and the pattern of Karmen Vortex Street got from his simulation with the relative results of previous researches. The identification of them means the reliability of his CFD model. Then the velocity profiles upstream the paper side filaments were observed. Uniform velocity profiles are expected to indicate uniform fiber distribution during the dewatering process and minimum drainage wire mark will be achieved. The location of the velocity profile was somewhat arbitrarily set to a quarter of the small filaments' diameter above the highest points of the small cylinders.

He got the standard uniform velocity profile when only the first cylinder row was evenly distributed in the domain. Then the second cylinder row which indicated the machine side of multi-layer forming fabric was added and the new velocity profile was checked. The variation of the profiles indicates the influence of the machine side filaments on the fiber uniformity of the detained sheet. Meanwhile, many geometric parameters such as the diameter ratio of the two rows D/d, the Z-direction separation of the rows Z, the second row spacing $G2$, and the offset between the two rows Y were tested (Please refer to Figure 2.1). The new profiles of each case were presented together with the standard profile to show the effect of fabric structure variation on fiber distribution.

The major conclusions of his research are listed below:

- When the forming fabric has fine mesh on both paper and machine sides, variation of geometric parameters has very slightly impact on the velocity profiles upstream.
- When the fabric has a fine mesh on paper side but coarse mesh on machine side, the Z-direction separation between the two layers has the most significant effect on the wire marking and there is a critical distance at which the adverse effect diminishes.
- Unequal CD separation of the machine side layer plays a negative role in wire marking.

In reality, fiber deposit on the forming fabric gives the porous paper sheet structure in three dimensions, so 3D model will definitely give a better simulation interface than 2D one. Three-dimensional fabric models, in the beginning, were often intended for prediction of mechanical properties [30]. As the next step, a series of very accomplished numerical models for forming fabric and fiber sheet were developed by C. Barratte, et al. [31, 32] Based on previous two-dimensional, straight line fiber mat simulation [33] and Givin's model [34], they focus on setting up the 3D structure properties and forming fabric input.

Their approach simulates what is happening to each fiber during forming process and calculates the final characteristics. The simulator describe the forming fabric as a woven structure with repeated pattern and a software called CyberFab has been developed for that specific

purpose. Fabric can be woven from 2 to 5 filaments, and filament diameters, as mesh count of each filament are requested to build a fabric. Moreover, plane difference of both the paper side and the machine side are introduced as parameters. Other input parameters needed for the model are the length and width of the forming fabric sample to be studied. Fibers themselves are described individually by its length, width, thickness, coarseness, orientation, and flexibility.

After modeling the forming fabric and fibers, the mechanical retention process is simulated to get the retained fiber sheet. This condensed fiber network is then characterized by the calculation of its papermaking related properties, such as basis weight, thickness, density, orientation, porosity, and roughness. It is believed that the surface topography of the fabric is of prime importance as it determines key interaction with the fibers. The forming fabric surface profile and the calculated sheet roughness can be derived from their code. They found that the flatter the profile, the smoother the surface and there are less occurrence of wire mark and paper roughness, which has a directly positive influence of paper printing and coating behavior.

Retention on the fabric and its propensity for not marking the paper are quantified by the computer program and optimal conditions to reduce wire mark and increase retention can be determined by their model. Numerical results show that porosity has more relation with the retention property of forming fabric. Besides, the model allows a prediction of some effects of fabric or furnishing characteristics changes on the formed sheet structure. Currently, their sample size is small and only micro-properties can be evaluated. However, the algorithms are expansible to bigger scale simulations, and the only bottleneck should be concurred is the computer capacity.

2.2.3 Industry methods

Besides scholar researches, industrial analysis methods have been well developed during these decades, which has become a necessary step of quality control in papermaking industry. Paper product surface and forming fabric topography can be well simulated and monitored, but till now industry can know the products surface quality only after their manufacture.

Voith Paper Fabrics is able to establish most critical factors necessary to provide the fibers the ultimate amount of support using three-dimensional surface topography technology [35]. They developed a modular, optical scanning profilometer to optimize as well as stabilize manufacturing processes. Once the fabrics are scanned using a confocal laser, they are then put into a complex software system and analyzed, displaying required results. Results can be shown using topographic views, profiles (2D), photo-realistic views or 3D projections. Since fabric surface topography is a result of the supporting fabric structure, fabrics can therefore be modified and enhanced in the development phase and lead to improved, smoother end products.

Weavexx is also doing this test with a laser-scanning tool called Weavexx Surface Analyzer, which is capable to measure the elevation of a spot on filament or felt surface [35]. The accuracy is up to 0.01 microns. Similar techniques have been applied in other companies such as AstonJohnson and Albany International.

2.3 Conclusion and objective

The comprehensive review of the plentiful literature shows that presently, scholars have well stressed the mechanism between the topological structures of forming fabric and the wire mark degree, either experimentally or numerically. But basically there is no research considering the wire mark characteristic when the forming fabric itself has an imperfect structure. More specifically, a possibility of this imperfection is that one or more filaments are displaced from their original position. This kind of geometric non-uniform defect of forming fabric can transpire either within its manufacture streamline or during the papermaking procedure.

A frequent source of this kind of structure destroy is the blades in forming section. In twin wire former, there are some blades in the static pressure elements. As the fabrics under tension pass over each blade, the static pressure between the fabrics is rapidly built around the blade vicinity, to counter the component of the fabric tension force acting normal to the blade [36]. This pressure buildup from these blades causes very rapid dewatering rate there, while at the same time they

can also inevitably scrape the fabric surface.

Intuitively, this imperfect geometry of forming fabric will disturb the vicinity micro geometric structure of detained fiber sheet which is drained on it. It possibly will afford an initial fiber mat with less uniformity than ideal forming fabric brings. From Danby's research [2], the uniformity degree of the initial fiber mat in fact influences subsequent layers of fiber as the sheet is formed. So under the worst estimation, even the larger scale formation of the paper sheet will become non-uniform as a result of this filament's displacement.

The purpose of this study is to build a three-dimensional forming fabric model and apply the modern computational fluid dynamic (CFD) technique to simulate the detailed dewatering process occurs on forming fabrics [37]. Not as previous research, a better insight of how the non-uniformity of forming fabric structure (filament's displacement) affects the sheet wire marking is specifically wanted. Wire marks have a direct relation with many quality aspects of final paper sheet, so the ultimate goal is to help design and maintain suitable forming fabrics to reduce wire mark level as well as improve the uniformity of paper sheet.

2.4 Approach and assumptions

2.4.1 Approach

A single-layer forming fabric was modeled in this study since all essentials of fabric research can already be involved. The simulation scheme is similar for forming fabrics with more complicate geometric structure which are actually widely applied in industry. The only concern for their modeling is the dramatically increasing requirement of computer capacity. Parallel processing of CFD software and/or multi-processor computer configuration becomes a necessity in those cases.

A 3D geometric model will be built on Unigraphics, a computer aid design (CAD) software package. Three-dimensional model can involve the effect of both MD filaments and CMD filaments. Thus, it can distinguish the different type of forming fabric and get more creditable

result than 2D model. The geometric model will be put into preprocessing software, Gambit, to generate compute node and hybrid control volume meshes. Commercial CFD software Fluent 6.2 is used to do the computational work. In the end, post-processing software, Tecplot, can be served to present the necessary results that are interested in.

The 2D/3D velocity plots a quarter of filament diameter above the highest points of forming fabric filament will be shown. It is based on the assumption of the fibers can perfectly follow the single-phase-flow streamlines and the three components of the fluid velocity represents the local fiber distribution of the paper sheet. For instance, non-uniform MD velocity profile indicates the non-uniformity of the fibers' distribution in MD. This assumption is highly valid because the fiber density or crowd number is very small and the fibers are so tiny that they do not alter the Newtonian fluid pattern. Pressure drop and mass flow rate will also be studied for reference.

Some previous researches [32, 38] brought porous medium concept into forming fabric modeling. However, porous medium model cannot reflect the detailed non-uniform structure of the forming fabric with filament's displacement and its influence on the fluid velocity profile. So this approach was finally denied.

2.4.2 Assumptions

The real time simulation of entire dewatering process above forming fabric is very complicate. As the first step, only the initial stage of fiber mat formation process will be simulated in this research. Initial dewatering stage has most direct interaction with forming fabric and can influence subsequent layers of fiber mat formation as the sheet is formed [2]. So current results is a decent foundation of further study, which maybe involves the growing fiber mat itself in the model.

Another simplification is that the fiber suspension is considered as a single-phase liquid water flow. This is based on the fact that the suspension sprayed out of the headbox is very dilute (0.1%-1%) [39], and the interaction between water and fibers is neglectable with a considerable accuracy.

In industry, during the initial draining process on forming fabric the Reynolds number is around 160 based on the diameter of fabric filaments and the flow velocity over it. From empirical knowledge, for this complex geometry, the status of the headbox jet striking the forming fabric is likely in the transition stage and is unstable. With the growth of fiber mat, the local velocity decreases and flow could become stable. In fact, after calculation and comparison in next chapter, it demonstrates that steady model and unsteady model afford highly identical results. So to save the computational resource, basically only steady status was selected. See chapter 3 for details.

Besides, laminar viscous model, rather than turbulence model, was used. The headbox jet impinged on forming fabric surface is turbulence with low turbulent intensity. Considering the concerned flow of this research is the drained pulp suspension moves in vertical direction, its status is likely to be laminar. Therefore, only laminar viscous model was selected.

In summary, the assumptions of this study are:

- The growing fiber mat in dewatering process is out of consideration.
- Fiber interaction is neglected and the flow is treated as single-phase water.
- Laminar flow is assumed for both steady and unsteady model.

In this chapter, firstly the concepts of formation and wire mark has been presented, and current researches about forming fabric structure, wire mark, and printing quality have been summarized. Then based on previous researches, the target and approach of this study were set up. In next chapter, the modeling method and model's validation will be illustrated.

Chapter 3

Modeling and Validation

The related background knowledge of papermaking industry has been discussed in pervious chapters. The scope, objectives, and approaches of this research have also been clarified. In this chapter, the three-dimensional CFD model of the forming fabric and its creditability will be discussed. The modeling schemes were validated with the data from a wind tunnel screen experiment [4] because the lack of experimental data for fabric itself. This validation is feasible because of the structure similarity between the forming fabric and wind tunnel screen. In the end, a CFD accuracy analysis using the method suggested by I. Celik [40] was applied for assuming the computational accuracy. Fabric with the simplest geometric structure, single-layer forming fabric, was modeled to save the computational time and resource. This scheme can be easily expanded to complex fabric with some modification of geometry structures.

It is hard to choose a suitable organizing order for this chapter because in practice different contents of CFD modeling overlap one another. Therefore, even an arbitrary order which is hopefully convenience for understanding was tried to be achieved, maybe the former sections will still have the pre-requirements which are actually shown in latter sections. But basically you can get a good comprehension after reading the entire chapter.

3.1 Modeling

3.1.1 Geometry modeling

The forming fabric modeled here is the top layer of 73*75 mesh forming fabric, one of the commercial triple-layer fabrics. As mentioned in chapter1, triple-layer forming fabric are combined by two relatively distinguish single-layer forming fabrics with bonding filaments. The top one of that fabric is the prototype of this study.

The three-dimensional geometry model was built by modeling modular of Unigraphics, a CAD software package, which is built on the base of Parasolid modeling kernel technology. Solid geometry model was exported from Unigraphics in Parasolid format and import into Gambit for getting computational meshes. Commercial CFD software Fluent 6.2 was used to do the flow field numerical calculation. Finally, post-processing software Tecplot was served for presenting the related 3D results. As the first step, only the initial draining stage was modeled, and the growing fiber mat during the drainage process was not included.

Real forming fabric suitable for industry production is usually a very huge component with approximately seven meters wide and tens of meters long. But it has a repeated wave pattern and consisted of small scale repeated units. So in fabric research, usually only one single repeated unit of fabric with periodic boundary conditions, which contains all the geometry information, is simulated. For instance, some researchers such as Timothy Waung and Green have done the modeling work within one repeated unit of a fabric [41]. However, since the specialty of the "imperfect" topological structure in this study, a area of one repeated unit in CMD by two repeated units in MD are needed to be involved in simulation domain. It is a necessity for showing the non-uniform fabric structure because arbitrarily, the middle MD filament shared with the two MD units was chosen to be displaced.

The isometric view of the calculation domain for the uniform fabric is shown in Figure 3.1. There are two kinds of areas in the domain: knuckles (filaments) and pores. Filaments orient in either MD or CMD. Single-layer forming fabric, which has the simplest sinusoidal wave pat-

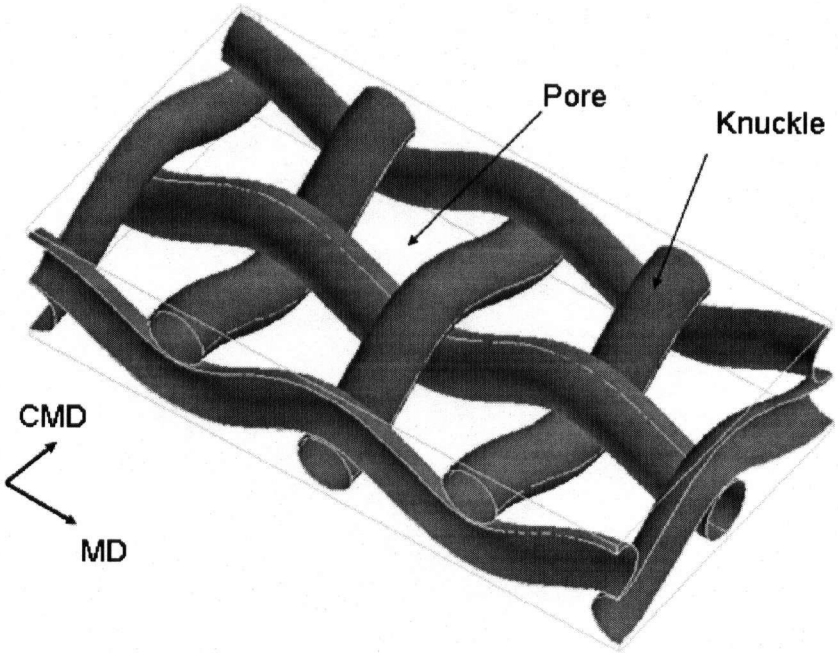

Figure 3.1: An isometric view of the calculation domain for the uniform fabric.

tern that repeated every two filaments both in MD and in CMD is under consideration. In other words, there are two filaments in each direction within every repeated unit. For presenting the displacement of filament, the calculation domain contains two units of that forming fabric along MD. Later the credibility of this model will be checked.

The modeling dimensions are from the data sheet of AstonJohnson, and applied by Zhaolin Huang in his research [3, 42]. The fabric filaments have different diameters in different directions (MD and CMD), but in this model the diameters are simplified to have an identical value D=0.13mm. The separation in both two directions is L=0.35mm. This simplification is to reduce the number of parameters show up in the problem, which can offer a step-by-step understanding in the first stage. Figure 3.2 shows the top view and front view of the fabric geometric structure marked with dimensions.

The filament with displacement was chosen in MD, so the results represent the surface non-uniformity in MD. The reason for this is that primly the blades in forming section will scrape the MD filaments during the dewatering process. CMD filaments' displacement will cause similar results as in MD. Combination of displacements in dual di-

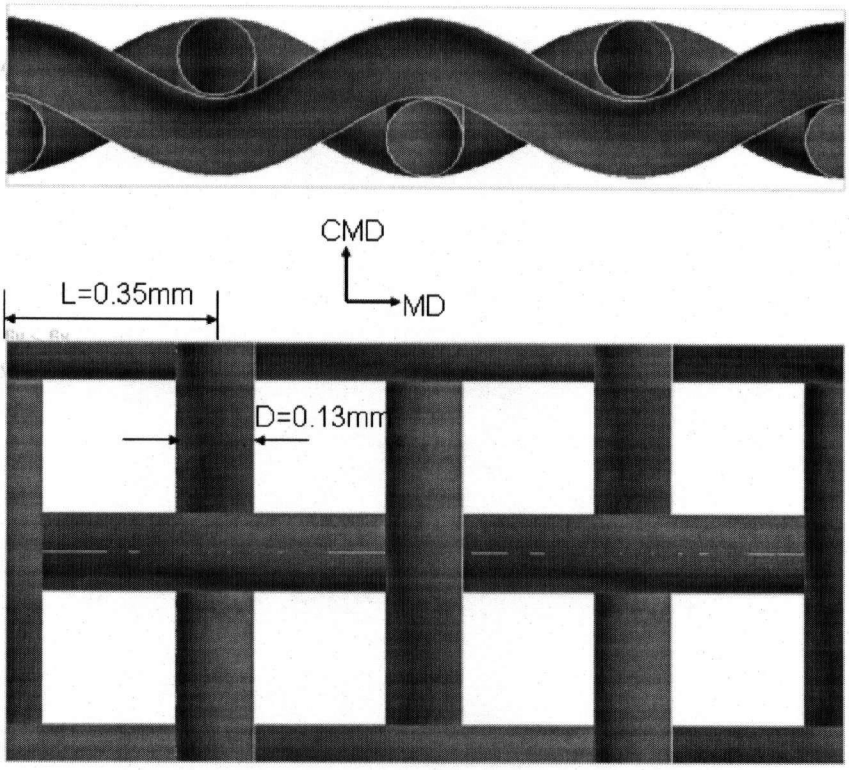

Figure 3.2: Top view and front view of the geometric structure of the uniform fabric.

rections was not involved in this thesis, because it rarely happens in reality and will lead to more complicate phenomenon which will block the fundamental things.

In cases of just one filament moves off its original location, the displacement varies from 5% to 30% of the normal filaments spacing, with an increasing step of 5%. The largest possible displacement is determined by the fabric geometric structure. When two or more filaments are displaced together, the displacement varies from -20% to 30%. Minus one means the movement is opposite the MD direction.

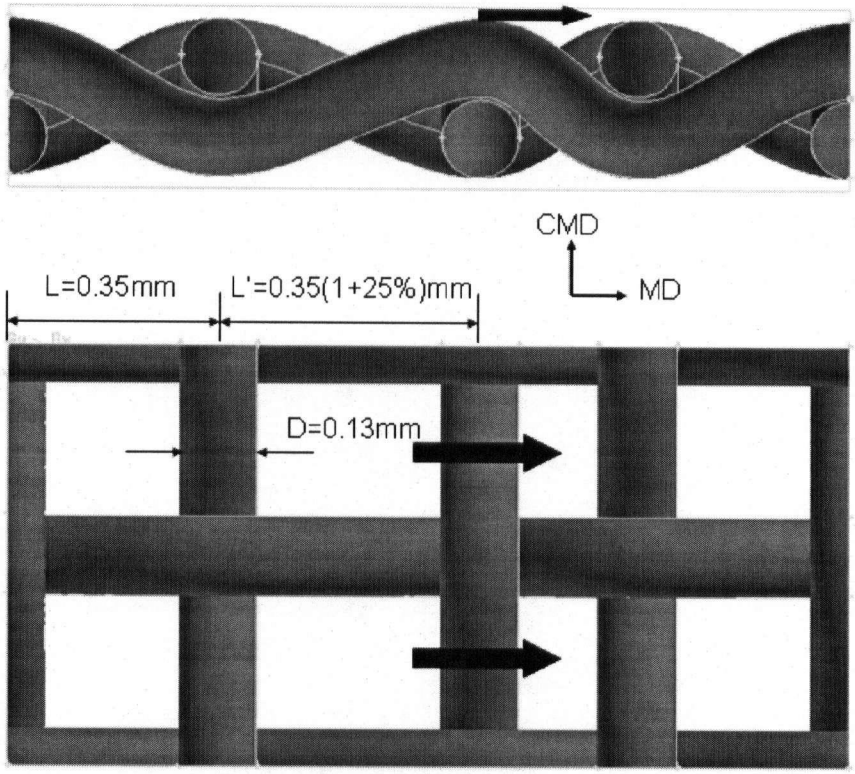

Figure 3.3: An example of the fabric geometric model with filament displacement. One CMD filament has a displacement of 25% filament spacing in positive MD.

Figure 3.3 is an example of the fabric geometric model with filament displacement. In this case, one filament moves toward positive MD with the displacement of 25% filament spacing. Note that with the filament's movement, the pores on its left become 25% larger and pores on its right is 25% smaller as well. The interaction between the displaced

and fixed filaments was also considered. The slope of the MD filaments at the contact point was restricted to be horizontal. This reflects the real deformation of the MD filaments when CMD filaments move.

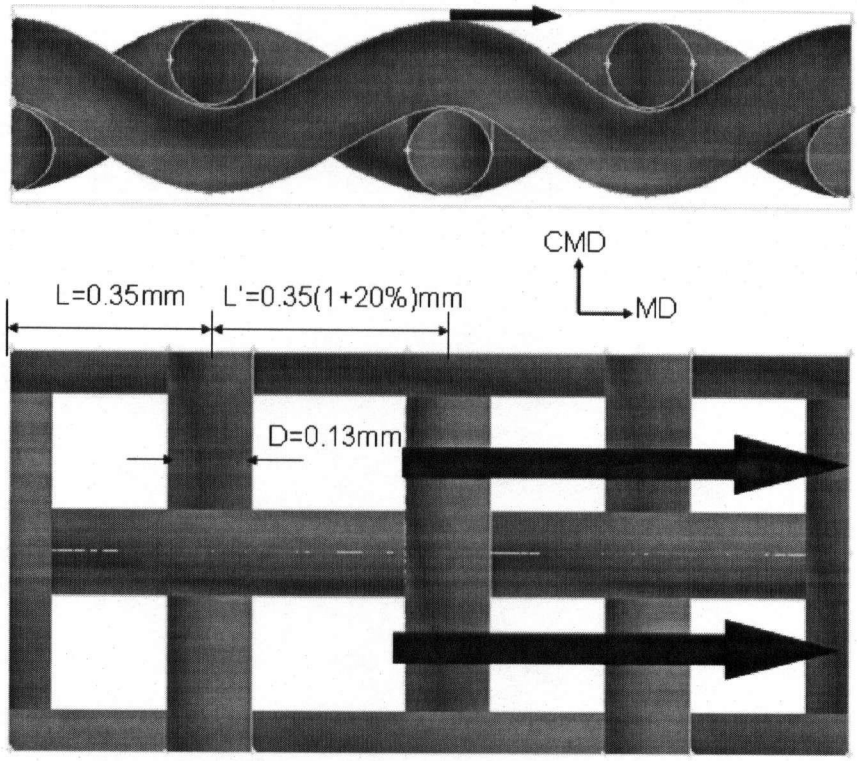

Figure 3.4: An example of multi-filaments move together. The right three CMD filaments are moved toward positive MD with a displacement of 20% normal spacing.

In Figure 3.4, the right three CMD filaments move together toward positive MD with a displacement of 20% normal spacing. Comparing with single-filament displacing cases, cases with multi-filaments displacement represent a heavier topological deformation of forming fabric, which happens when more than one filament are dislocated by forming blades. Note that only the pores left to displaced filament is enlarged, while the size of pores right to it do not have any change.

3.1.2 Grid generation and grid convergence

After modeling the geometry of forming fabric, next is to generate a computational mesh scheme suitable for calculation and with fast

convergence. Sometimes grid generation is a very headache problem of CFD application. For this fabric model, size function in Gambit was used as a convenience tool to get a suitable and tunable mesh scheme. Then grid convergence, or gird independence named by some literature, is checked.

3.1.2.1 Grid generation

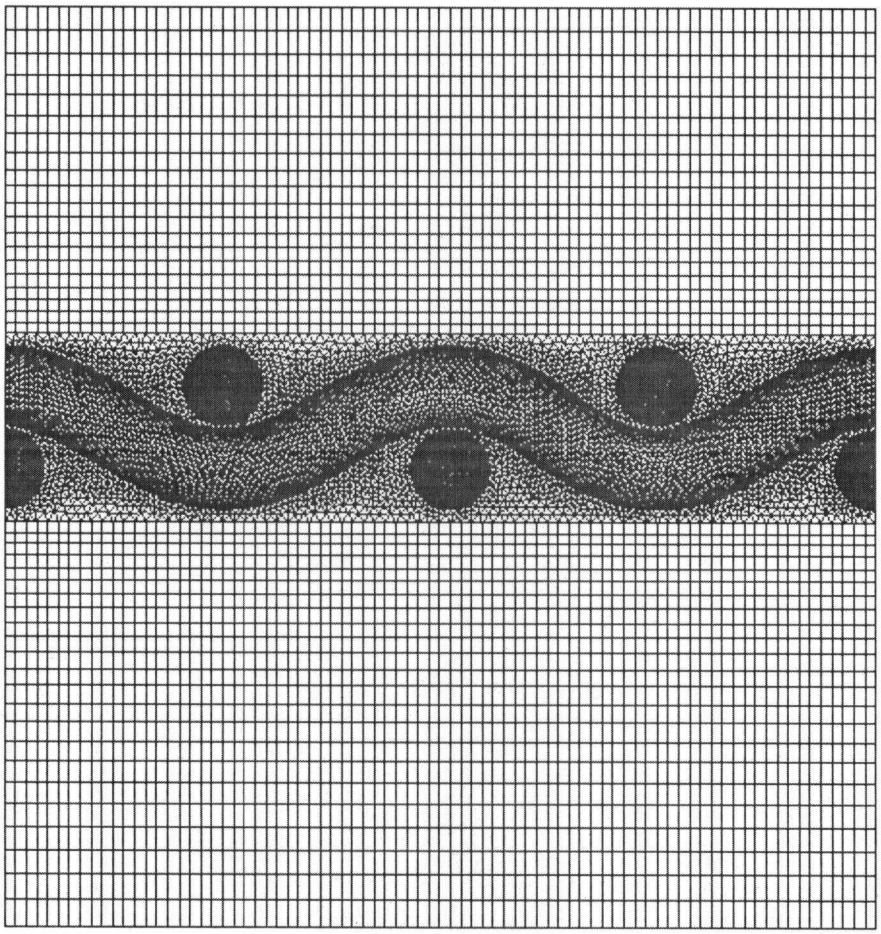

Figure 3.5: Hybrid computational mesh scheme applied in this research.

As shown in Figure 3.5, there are three sections in the calculation domain: inlet area, outlet area and fabric area. Inlet and outlet areas of the domain are introduced to guaranty the velocity inlet and pressure outlet boundary conditions are applicable. Hybrid mesh scheme is applied as a compromise of the geometric complexity of fabric area and the over all computational expense. Structured mesh has a faster convergence, but hard to be applied in fabric's complex geometric struc-

ture. So structured mesh was applied for inlet and outlet areas, and unstructured mesh was applied in fabric area.

Size function tool was applied to generate the unstructured mesh in fabric area. The source and attached surface of each size function is the centerline of each filament and the filament surface, respectively. The over all grid size can be controlled by tuning the start size, growth rate and size limit of each size function, which is a necessity to check the grid convergence. Successive ratio scheme of edge meshing was applied in structure mesh generation to reduce the unnecessary computational work meanwhile keep high calculation accuracy where it needs.

3.1.2.2 Grid convergence

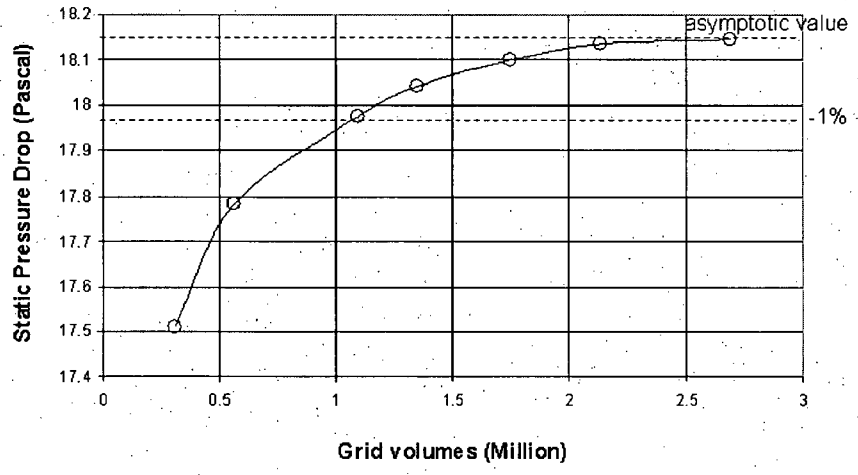

Figure 3.6: Pressure drop results of the case with 5% spacing displacement, under seven different grid sizes.

Grid convergence will be achieved when the calculation keeps steady with the increasing of grid size. Suitable grid size should be decided to gain enough accuracy with lowest computational expense. Up to seven different grid sizes with geometric similarity were achieved to check the grid convergence, which is realized by simply changing the parameters of the size function. The pressure drop results of the case with 5% spacing displacement, under seven different grid sizes, are gathered in Figure 3.6. The result of the grid scheme with slightly over 1 million grid volumes already falls in 1% of the asymptotic value, which

usually means "accurate enough" [43]. Simulation cases with different displacements show the similar behavior. Therefore, a grid scheme with approximately one million grid volumes is the final selection of this study.

Table 3.1: Pressure drop values and point velocities of five different grid sizes.

Grid Size (million)	0.307	0.565	1.094 (applied)	1.749	2.689
Pressure Drop (pa)	17.51	17.78	17.98	18.09	18.14
Max Peak Velocity (m/s)	0.05534	0.05507	0.05535	0.05529	0.05524
Min Peak Velocity (m/s)	0.04950	0.04890	0.04908	0.04905	0.04901

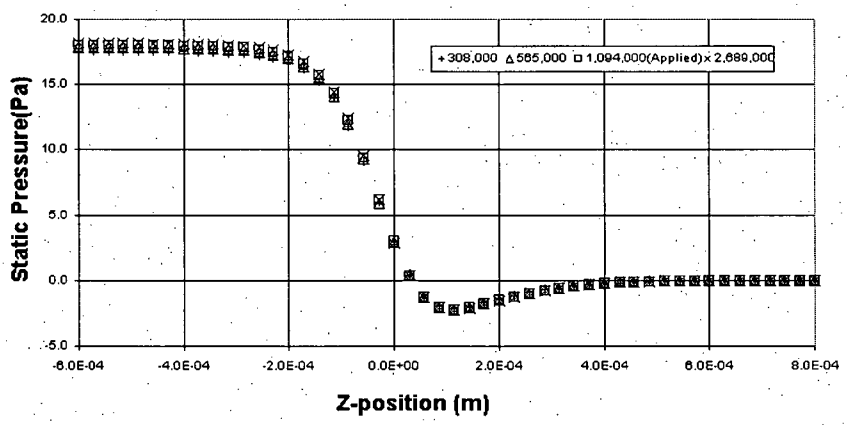

Figure 3.7: Pressure distributions along the Z-direction of the forming fabric of four different grid sizes.

Table 3.1 gives some pressure drop values and point velocities of five different grid sizes. Figure 3.7 shows the pressure distributions along the Z-direction (vertical to fabric plane) of the forming fabric of four different grid sizes. It is demonstrated that all monitored parameters keep within the scope of 1% of the asymptotic value when the selected grid size is applied, which also verifies the grid size selection of this study.

3.1.3 Geometric model validation

Geometric modeling strategy has been discussed in previous sections. Only a domain of two repeated units along MD is calculated and periodic boundary condition is applied. Then the problem is that the

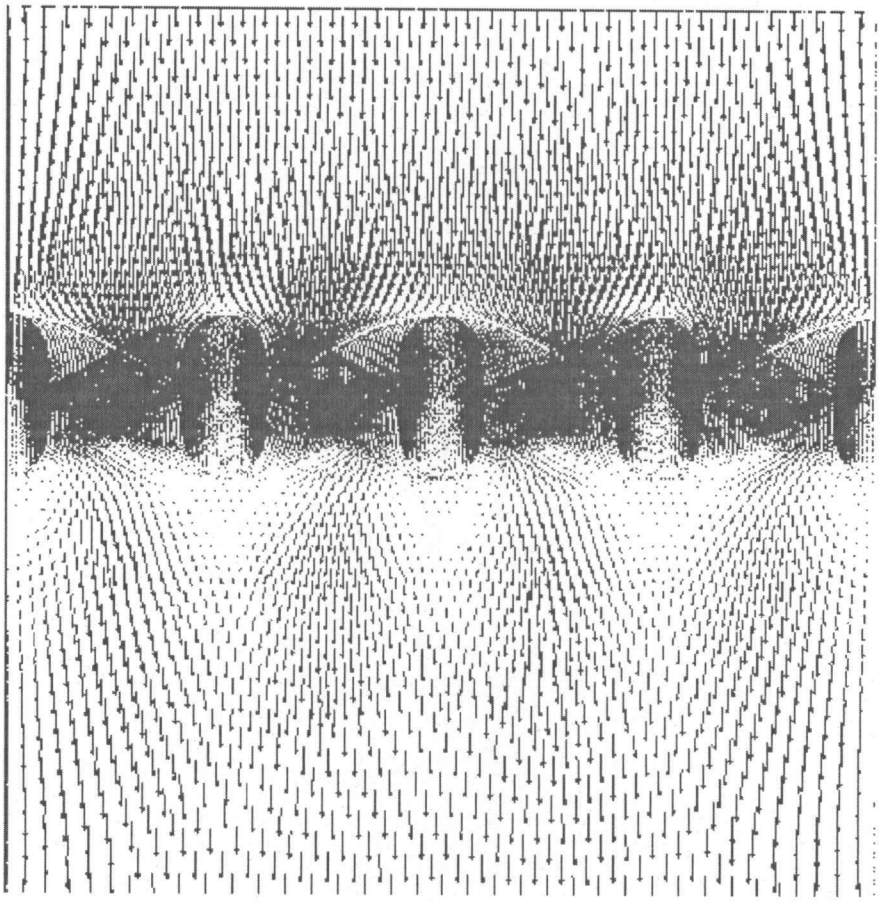

Figure 3.8: Velocity vector plot of the calculation domain.

filament displacement within the domain will be duplicated by the periodic boundary condition and broadcast to every repeated unit of fabric, which actually will not happen in reality. However, from Figure 3.8, velocity vector plot of the calculation flow field, it is obvious that the vectors go through the domain from the inlet to the outlet largely in a straight way. The local displacement of one fabric filament will not make any difference on the flow field two repeated units away. This means whether the filament two units away is displaced or not, the local velocity will keep the same. Now it is safe to say that the results will have no difference with the results from the fabric model that only has local filament displacement. In other words, this model can describe the real problem and the domain size is enough for the application of periodic boundary conditions.

The suitable depths of the inlet and outlet area were also determined by numerical trials. The depths should be as short as possible to achieve the most computationally economic simulation, under the condition that the results have no significant difference since the variation of the domain depths. Finally, the domain depths were reduced from 15 filaments diameter (D) for inlet area and $20D$ for outlet area to $4D$ and $5D$, respectively. The results varied within 0.5% for above two cases.

3.1.4 Solver selection and settings

3.1.4.1 Solver selection

A commercial CFD software, FLUENT, was used in this simulation. FLUENT uses a control-volume based technique [44] to solve the continuous equation and integral N-S equations for mass and momentum conservation, respectively. Control volume technique integrates the governing equations on every control volume, yielding discrete equations that inherently satisfy the mass and momentum conservation on a control volume basis. Since turbulent models and heat transfer effects were not included, no scalar equation was involved in the equation set. The governing equations are converted to algebraic form that can be numerically solved by the solver. Then the equation set consisting the equations of every control volume will be solved iterately.

Since the flow can be treated as low speed incompressible fluid, a segregated solver was applied, i.e., the governing equations for every variable were solved sequentially. For segregated solver, implicit equation set solving methods which once solve one variable (such as u velocity) in the entire flow field is the only way for iteration. Fluent uses Gauss-Seidel method [44] to solve this equation set combined by equations of all computational cells, each cell has one equation.

In this sequential procedure, the continuous equation is used for solving the pressure field. Standard pressure interpolation scheme was selected because of the fluid's incompressibility. Considering the pressure-velocity coupling method in the segregated solver, SIMPLEC (Semi-Implicit Method for Pressure-Linked Equations-Consistent) [44, 45] and PISO (Pressure-Implicit with splitting of Operators) [44, 46, 47] methods were selected for steady and unsteady model, respectively. Both of them belong to SIMPLE algorithms [44, 48], which introduce the pressure item into continuity equation. SIMPLE algorithm family uses a relation between velocity and pressure corrections to enforce the mass conservation and then obtain the pressure field.

Besides, second-order upwind scheme was applied for momentum equations to achieve decent accuracy. Standard scheme is good for the pressure equation of low speed incompressible flow. Second order implicit time advance scheme was used to simulate unsteady flow, which can guaranty high-accuracy time resolution as well as keep numerical steady of the simulation.

As mentioned before, one major simplification of this study is considering the fiber suspension as a single-phase liquid water flow. This is based on the fact that suspension sprayed out of the headbox is very dilute (0.1%-1%) [39], and the interaction between water and fibers is neglectable under a considerable accuracy level. This model is only for the initial stage of the dewatering process, which has a significant impact on final fiber mat [2]. So the growing fiber mat during the process is not involved.

Although the headbox jet impinged on forming fabric surface is turbulence, its turbulent intensity is relatively low. Also, considering the

concerned flow of this research is the drained pulp suspension moves in vertical direction by gravity effect, its status is likely to be laminar. So as a first step, only laminar viscous model was selected. This conclusion should be verified by experiments. If it shows that the drained flow is turbulence, then turbulence models should be applied in further studies.

For the discussion about steady or unsteady modeling, see next section.

3.1.4.2 Steady and unsteady

To discuss the flow status during the dewatering process, firstly the local Re number should be calculated. The local Reynolds number based on the diameter of forming fabric filament is given by Equation (3.1):

$$Re = \frac{\rho \cdot U \cdot D}{\beta \cdot \mu} \tag{3.1}$$

where

ρ = water density
μ = viscosity coefficient of water
β = open area ratio
U = incoming velocity
D = filament diameter

For the initial drainage process in papermaking industry, the typical dewatering velocity vertically going through the forming fabric by gravity effect is around 0.5m/s. The open area ratio β of selected forming fabric, defined as the ratio of planar area not blocked by filaments to total area, is calculated by Equation (3.2):

$$\beta = \frac{(L - D)^2}{L^2} \tag{3.2}$$

where

L = spacing between two parallel filaments
D = filament diameter

For this case, L=0.35mm and D=0.13mm, so β is around to 0.40. Based on above calculation, the local Re number of this study is around 160.

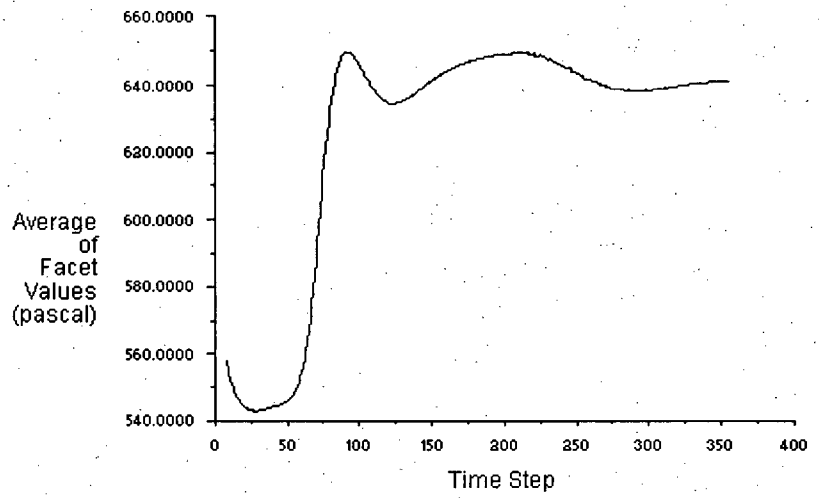

Figure 3.9: Fluctuation of static pressure on certain point in unsteady case.

Currently, there is no available experimental study on the stability of flow pass forming fabric model. But there are numerous researches on the stability of flow passes cylinders [49, 50, 51]etc.. From fluid mechanic empirical knowledge, the flow will become unsteady when the Re number is over 150 for the case of flow pass one cylinder [51]. For more complex structure such as forming fabric, the transit threshold would be much lower. So the initial stage of dewatering process is likely to be unsteady. It was tested by the result from unsteady simulation model. Figure 3.9 shows the fluctuation of the static pressure on certain point, which demonstrates that the flow field is unsteady indeed.

With the growing of fiber mat, it blocks most open areas of forming fabric and in the later stage of drainage process the local dewatering velocity typically decrease to around 0.05m/s, one-tenth of the initial velocity. So in steady cases, the velocity was set to 0.05m/s, and the local Reynolds number then changes to around 16. In this case, the flow field is largely steady from the empirical estimate. This guess was verified numerically and the test was conducted in an unsteady way. In other words, the inlet velocity was set to be 0.05m/s, but unsteady

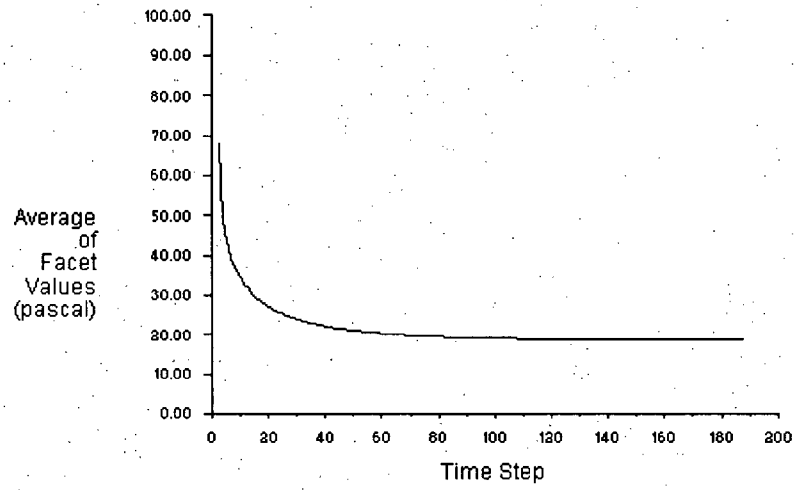

Figure 3.10: The variation history of static pressure on certain point in steady case.

solver was still selected. The result of the monitored variable, static pressure on certain point, is shown in Figure 3.10. It kept steady with the increase of the time steps, which confirms the flow field is steady in the later stage of dewatering process. However, this conclusion should also be verified by experiments.

The results of both steady and unsteady cases are put together for comparison. Figure 3.11 is the 2D velocity profiles of the case with 5% displacement. The location of the data rake will be illustrated in next chapter. The abscissa axis is the number of the CMD filaments, and five vertical guidelines represent the centerline locations of the CMD filaments. In this case, the centerline of the third CMD filament moves 5% of normal filament spacing to its right side. Ordinate axis is velocity normalized by the uniform inlet velocity. The data from the unsteady case are time-averaged value. In this figure, there is no significant difference between steady and unsteady profiles, which means the steady case can reflect the relation between filaments' location and velocity profile of the real unsteady problem. So to save computational resource, rather than using turbulence models, basically only steady cases were conducted in this research.

3.1.4.3 Boundary conditions

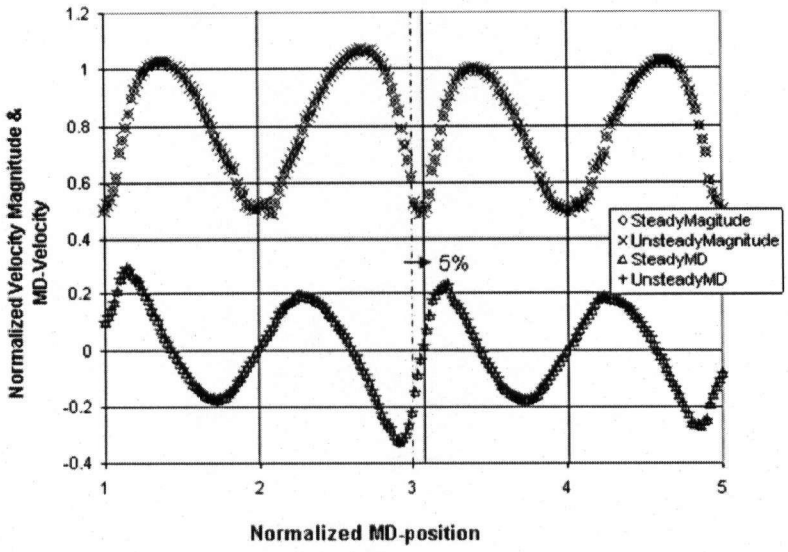

Figure 3.11: Comparison of velocity profiles from steady and unsteady model.

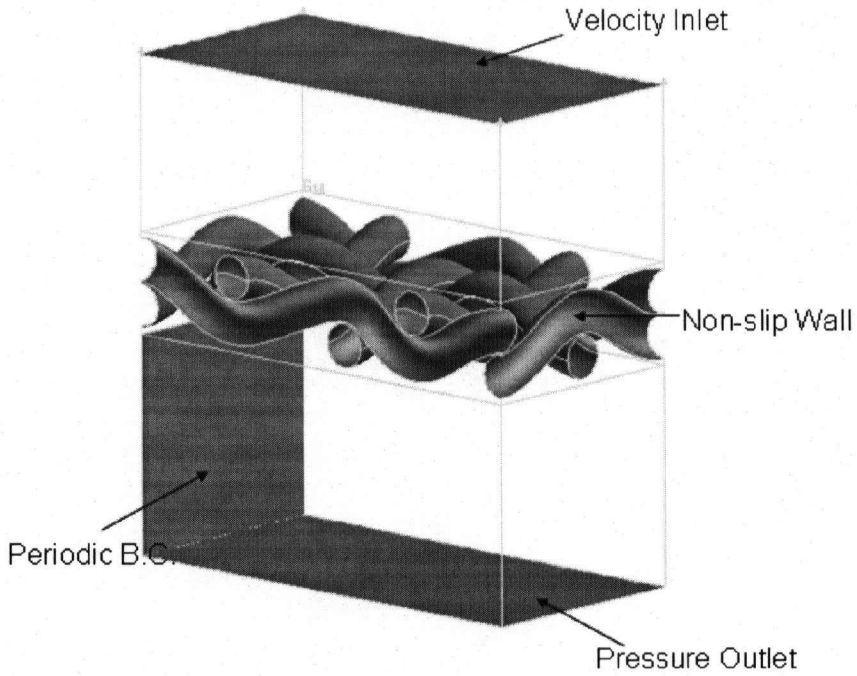

Figure 3.12: The boundary conditions of the domain.

Next concern is the boundary conditions. Firstly, velocity inlet with perpendicular uniform velocity was assigned for the inlet of the domain. This is because the fiber suspension gain the same velocity as the moving forming fabric right after the attachment, and the relative velocity in MD is zero. Only the vertical velocity component of water induced by gravity exists during the dewatering process. Then pressure outlet was applied and the gauge pressure in the center of the outlet plane keeps zero. Periodic boundary conditions were applied for all the domain side-walls, because of the inherited repeating pattern of forming fabric. Finally, non-slip wall type was selected for the filaments surface. The dimensions of forming fabric filaments is still one order higher than the scale suitable for micro-fluid theory in which non-slip condition is not satisfied any more [52]. Meanwhile, considering the fluid media in this study is water, a fluid with very small molecule size, the non-slip wall boundary condition can be safely applied.

Figure 3.12 shows the boundary conditions of the domain. Note that to facilitate the vision, only one side-wall of the domain is presented.

3.2 Iteration convergence judgment

There are three major criteria to judge the iteration convergence:

- At least three orders of magnitude decrease in the normalized residuals for each equation solved is achieved.
- The monitored variables keep steady for at least 50 iterations.
- The inlet and outlet mass flow rates are identical.

All this criteria was checked in this study. For time-dependent cases, iterative convergence at every time step was checked.

Figure 3.13 is a typical residuals plot of a steady case. It can be observed that all the residuals have a more than three order decrease on magnitude and then keep steady. The residual of continuum equation is stable at 10e-6, and those of momentum equations are stable at 10e-8.

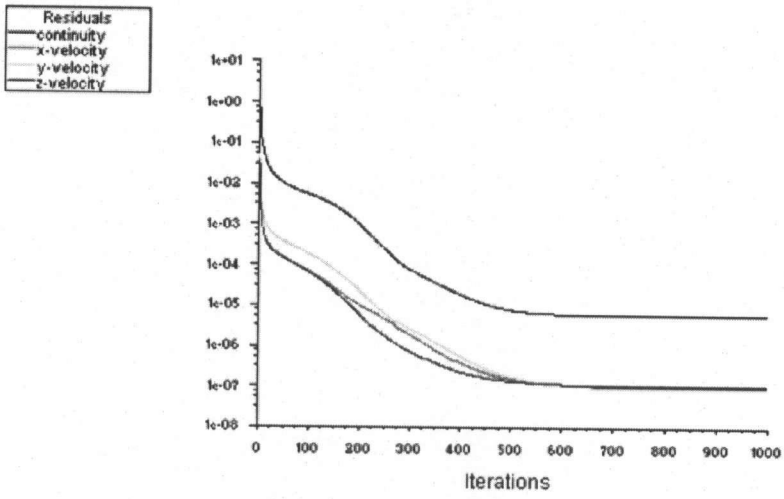

Figure 3.13: A typical residuals plot of a steady case.

Table 3.2: Mass flow fluxes of inlet and outlet and the net mass flow flux.

Inlet (kg/s)	4.89E-05
Outlet(kg/s)	-4.89E-05
net mass-flow-flux(kg/s)	-3.64E-12

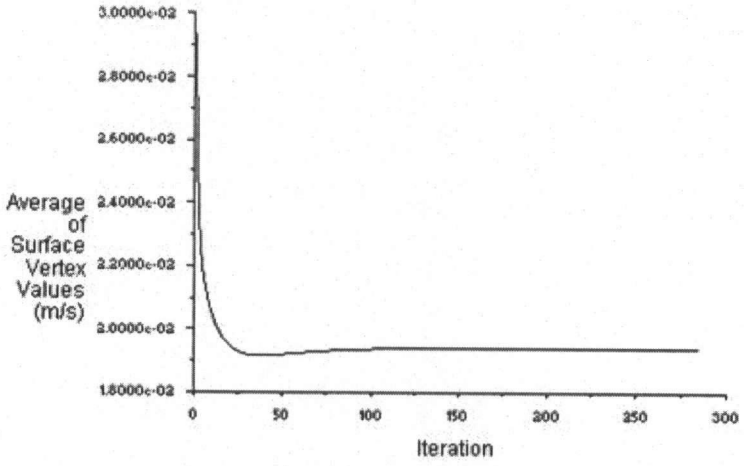

Figure 3.14: The variation history of velocity magnitude of certain spot in the flow field during iteration.

Table 3.2 shows the mass flow fluxes of inlet and outlet and the next mass flow flux. The net mass flow flux is infinitesimal and less than 0.0001% of the inlet mass flow flux, so the mass flow conservation is reached.

The criterion about the stability of the monitored variables was also achieved. Figure 3.14 shows the variation of velocity magnitude of certain spot in the flow field during the iteration. The velocity has already been steady after less than 200 iterations.

In summary, all the criteria for iteration convergence are satisfied. The iteration convergence was achieved in every CFD case of this study and the results are credible.

3.3 Accuracy analysis

An accuracy analysis of the numerical results was also conducted. I.Celik [40] recommended a standard accuracy analysis procedure that fits most engineering cases, basing on previous uncertainty estimation documents by Roache et al. [53] and their follower Freitas [54]. The method for discretization error estimation is the Richardson extrapolation (RE) or Grid Convergence Independency (GCI) method [55, 56], which is a widely acceptable method that has been evaluated over several hundred CFD cases. Following the procedure, the accuracy of this fabric numerical study can be roughly estimated.

To apply this method, the grid and iteration convergence must be checked as preliminary works. Then at least three set of grids with significantly different grid size should be built. The grid refinement should be done systematically, that is, the refinement itself is geometric similar even if the meshing scheme is hybrid. This is to guarantee the corresponding cells of different grid sets are roughly geometrically similar. It can be realized by the tunable parameters of the size function in Gambit. The detailed procedure of the GCI method is in appendix A.

The accuracy result for pressure is 3.0%. For velocity, the accuracy is 1.9%. These conclusion only takes consider of the truncated error of

the CFD application and doesn't account for modeling and round off errors. Since the major concern of this study is the comparison of the velocity plots of the uniform fabric structure and after the filament's displacement, which have the same accuracy, it is not necessary to include the error bars in the plots.

3.4 Wind tunnel screen validation

Since currently there is no 3D experimental research available on the detailed dewatering process in forming section, considering the dimensional and geometric structure similarity between wind tunnel screens and forming fabric, wind tunnel screen experiments data were served as the experimental validation of the CFD scheme applied in this forming fabric research. The numerical scheme used in this study will be duplicated to the simulations of wind tunnel screen. If the latter simulation is valid by relative experimental data, the numerical method used in former simulation should be indirectly validated. Table 3.3 shows the geometry dimensions of the NACA wind tunnel screens and forming fabric used in research. The dimensional similarity of them is clear.

Table 3.3: Geometry dimensions of tested forming fabric and NACA wind tunnel screens.

	Filament diameter (mm)	Separation spacing (mm)
Tested Forming Fabric	0.13	0.35
Screen B(NACA)	0.19	1.06
Screen C(NACA)	0.43	1.27
Screen F(NACA)	0.14	0.47
Screen D(NACA)	0.18	0.64

In wind tunnel study, screens were used to reduce differences in mean speed in order to obtain a more uniform stream. Meanwhile, they can also effectively reduce the turbulence, which is a necessity for many wind tunnel investigations [4]. Much importance was therefore attached to the wind tunnel screen and there were many experimental researches of it. One of these researches about the screen resistance will be used for the validation purpose.

Screen resistance is a very important character related with the energy diffusion. The resistance is usually expressed in terms of the screen pressure-drop occurring when a screen is in a duct with its plane perpendicular to the flow. The screen pressure-drop coefficient K and Low Reynolds number pressure-drop coefficient K^* are defined by Equation 3.3 and Equation 3.4:

$$K = \frac{\Delta P}{0.5\rho U^2} \tag{3.3}$$

$$K^* = \frac{\Delta P}{\mu U/D} \tag{3.4}$$

where

U = upstream velocity
ΔP = Pressure drop
ρ = water density
D = characteristic scale of the flow field

Since flow through a screen can take place only in the spaces between wires, K and K^* depends on its solidity, defined as the ratio of closed area to total area. Besides, they also vary with the local Reynolds number.

Many experimental studies have been done on the relation between pressure-drop coefficient and Reynolds number for different wind tunnel screens. Figure 3.15 shows one series of experimental data from G.B.Schubauer et al. [4]. The experimental data in Figure 3.15 were used to compare with the pressure-drop from numerical simulations, which are applied the same scheme as this forming fabric study. In numerical study, pressure drop values are the difference of the gauge pressures in front of and behind the forming fabric.

The error of the NACA experimental data at lowest velocity was estimated. The pressure drop coefficient K is determined by Equation 3.4. So, the error is mostly related to error of pressure drop and air velocity. But in their pitot-static tube experimental method,

$$\Delta P = \rho g h \tag{3.5}$$

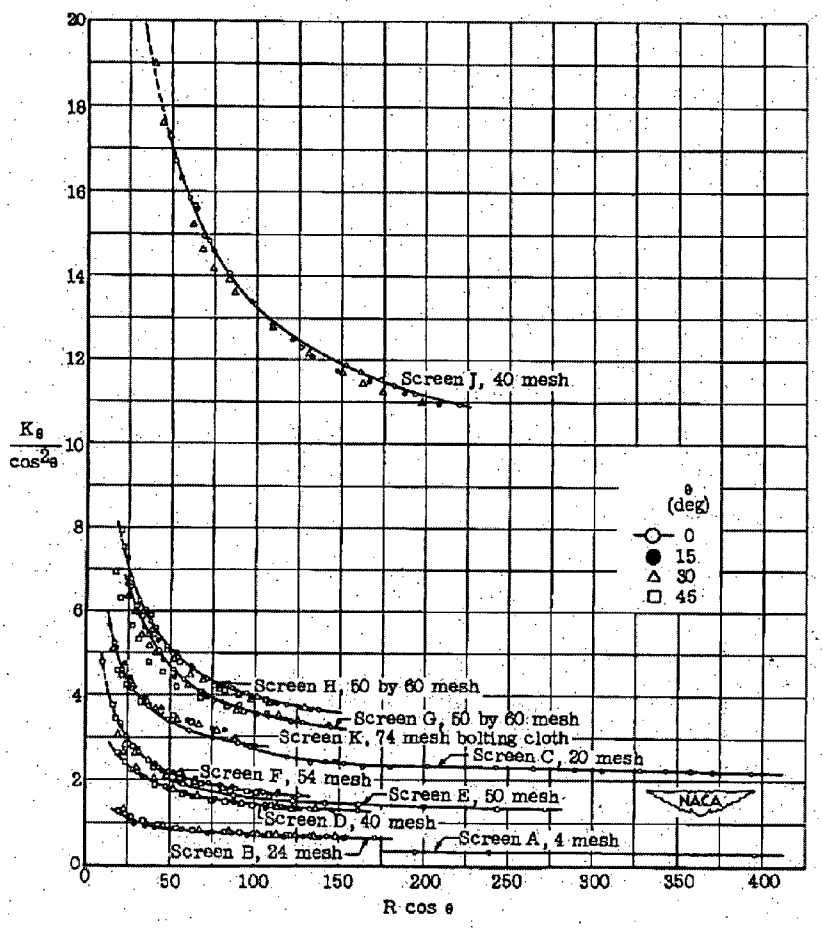

Figure 3.15: Pressure-drop coefficients for flow incident at angle θ and freely deflected by screen. All curves are drawn for θ=0° [4].

assuming the error of gravity accelerate and air density is very small that could be neglected, the only error source of pressure drop comes from the water height h, which is 22% under the experimental condition with small velocity. So, the error of pressure drop is around 22%.

From the error formula and the relation of pressure drop and velocity,

$$\Delta P = 1/2\rho V^2 \tag{3.6}$$

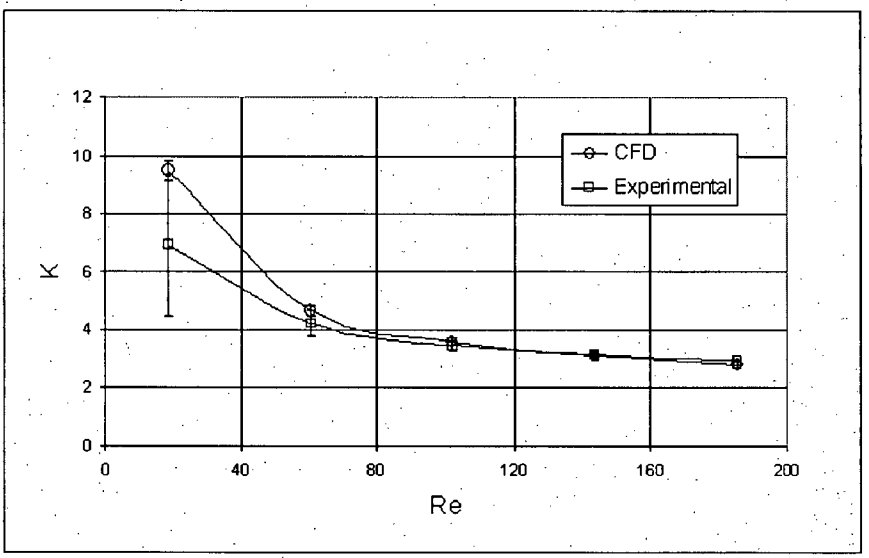

Figure 3.16: Comparison of CFD and experimental results of pressure-drop coefficient K as a function of local Reynolds number.

the error of V is around 17%. Then the error of K derived from Equation 3.4 is around 35%. Errors of other experiment data point can be derived follow the same procedure.

Figure 3.16 shows the comparison of the results of Screen H. Re is the local Reynolds number, which is calculated by the fabric's local velocity and the filament diameter. The derived error values for both experimental and numerical data are shown as error bar of each data point in the figure. The numerical results are generally fit the experimental data very well at high Reynolds number (Re >60). It indicates that the numerical scheme of wind tunnel screen study, hence that of forming fabric study is valid. At low Reynolds number (Re <60), there is a

roughly 40% discrepancy between the experimental and numerical results. This is because the local velocities in these cases are very small, and then K will be very sensitive to the error of the pressure drop from Equation 3.4. Besides, the pressure drop data of the experiments are only several tens of Pascal, which needs to be probed by pressure devices with very high accuracy. Previous error calculation shows, the error of the experimental data in that area is huge. Therefore, the data discrepancy in low Reynolds number area is contributed to the inaccurate measurement during the experiments.

In this chapter, the CFD scheme of this study has been thoroughly introduced, evaluated and validated. In Chapter 4, the related results will be illustrated and discussed.

Chapter 4

Results and discussion

In this chapter, CFD results of various fabric geometry cases will be presented and discussed. The results include detailed velocity 3D contours, 2D profiles, and pressure drops through the fabric as a function of the filament displacement. In addition, the mass flow rate through different fabric pores is presented.

4.1 Velocity distribution

As mentioned previously, an assumption of this study is that pulp fibers perfectly follow the single-phase-flow streamlines. So, the velocity distribution in the frontal vicinity of the forming fabric will be related to the fiber distribution in the finished paper sheet. In this section, 3D plane velocity plots and 2D rake velocity plots will be shown. The former provides a direct view of the velocity distribution in space, while the latter affords easier quantitative comparisons. The velocity magnitude and the MD velocity component will be shown to emphasize the general and detailed influence of the filament displacement, respectively. The major reasons of choosing MD velocity are that the displaced filaments are in MD and the fibers are highly oriented in MD in headbox therefore MD velocity is important for the uniformity of fiber sediment. The CMD velocity component is meaningless when the displaced filaments are in the MD. The Z-direction velocity data is very similar to the velocity magnitude since its value is 4-6 times higher than the other two velocity components. Therefore, the CMD and Z-direction velocity components will not be discussed. Before presenting velocity distribution graphs, data acquisition method will be illustrated.

4.1.1 Data acquisition

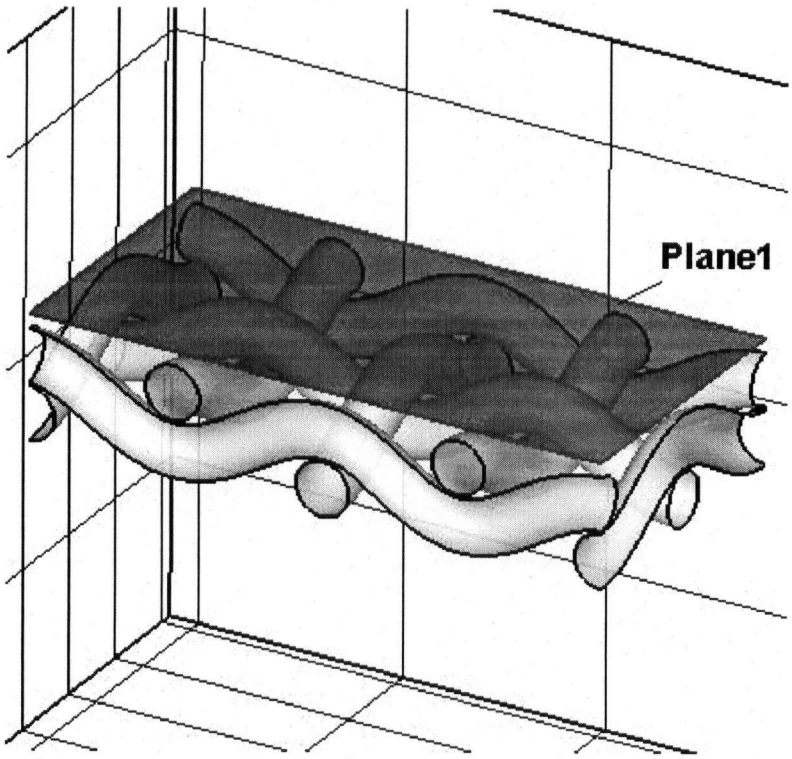

Figure 4.1: Location of the sectional plane (Plane 1) used in data acquisition for 3D velocity plots.

To present the detailed velocity distribution, a cross-section normal to the z-direction, in the vicinity of the fabric filaments, will be extracted. The velocity data within this sectional plane will be checked and compared. The location of this plane was somewhat arbitrarily set to a quarter of the filaments diameter ($1/4D$=0.0325mm) above the highest points of the forming fabric. This location is approximately where the fiber sheet formed in reality and should give a rough indication of the flow that is relevant to wire mark. Figure 4.1 shows this sectional plane, Plane 1.

Although a plot of velocity distribution in Plane 1 offers a very visual image of the detailed velocity distribution ahead the forming fabric, rake velocity profiles taken at different locations provide more readily quantifiable description of the flow. The velocity distributions along two rakes within the extracted sectional plane were used in these quantitative studies. Figure 4.2 shows the locations of the two rakes taken

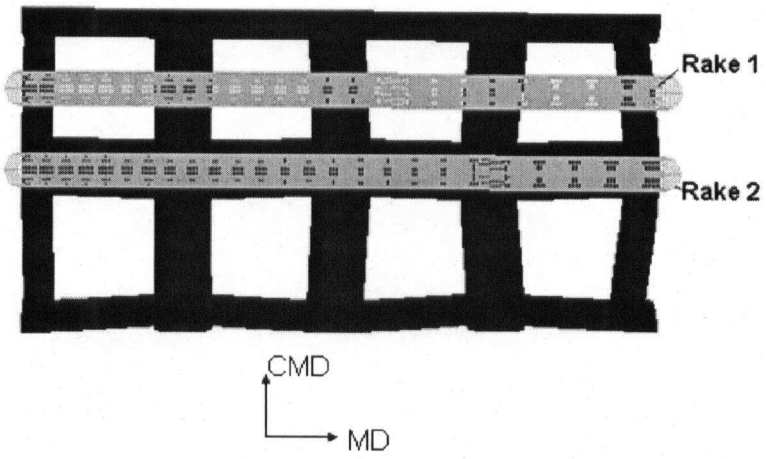

Figure 4.2: Locations of Rake 1 and Rake 2 using in data acquisition for 2D velocity plots.

from Plane 1, Rake 1 and Rake 2. Both rakes cover the entire MD of the calculation domain. Their locations differ only in their CMD. Rake 1 is above the center of forming fabric opens, while Rake 2 is just over the center filament in the MD of the domain. Rakes on these two typical spots can provide all required velocity information. Each rake has two hundred uniform-distributed data points. The velocity on these points will be presented in 2D scatter plots.

4.1.2 Plane velocity results

Figure 4.3 and Figure 4.4 illustrate the velocity magnitude contour at Plane 1 for the case when the filament structure is uniform. The three axes in Figure 4.3 are the real space coordinate: MD (machine-direction), CMD (cross-machine direction) and Z-direction. Both the isometric view and top view are displayed. The surface plots are colored by the velocity magnitude. From cold colors to warm colors, the velocity magnitude increases. In other words, as the color passes from blue to green to red the local velocity magnitude increases. All the other plots will use the same coloring scheme as Figure 4.3. Figure 4.4 is another three-dimensional velocity surface plot at Plane 1. The X-axis and Y-axis are the same as in Figure 4.3, but now the Z-axis parameter is the velocity magnitude in Plane 1. For a better understanding, the shadow of the forming fabrics is also shown.

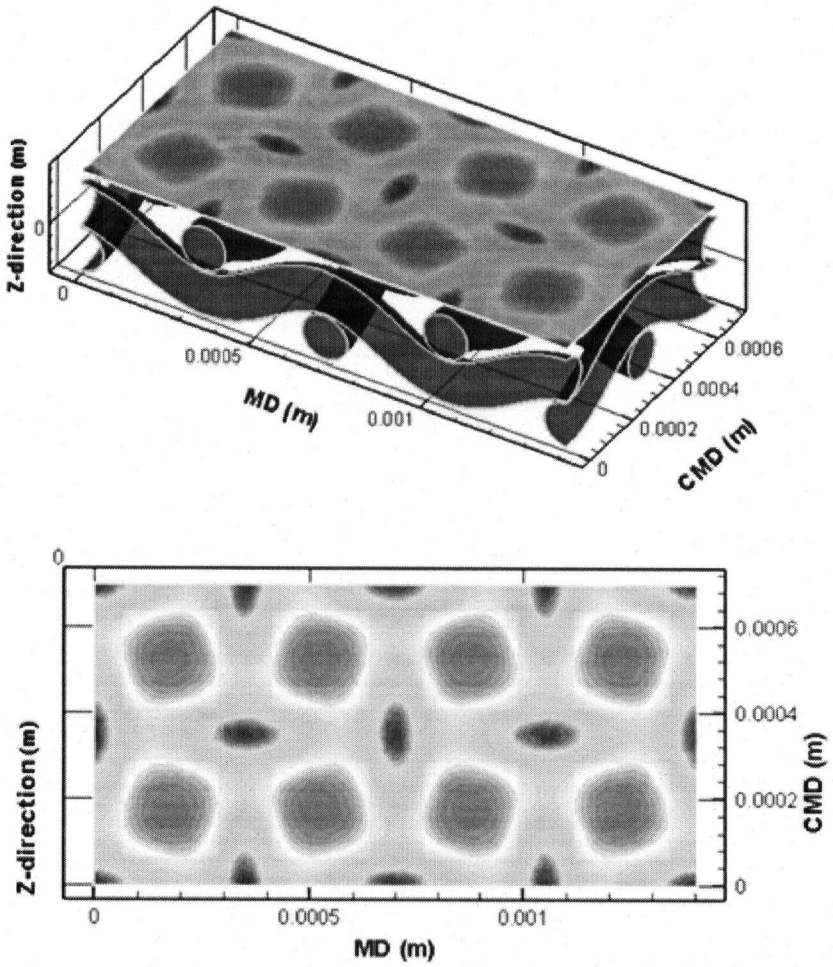

Figure 4.3: Isometric view and top view of the velocity magnitude contour at Plane 1, uniform mesh case, real space coordinate system.

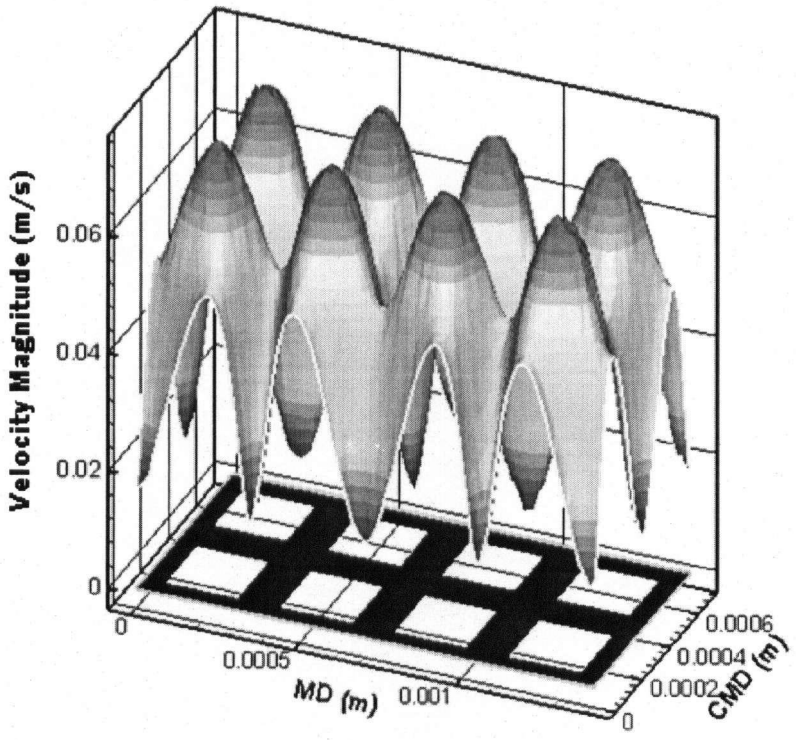

Figure 4.4: Isometric view of the velocity magnitude contour at Plane 1, uniform mesh case, Z-axis is the velocity magnitude in Plane 1.

In this uniform fabric mesh case, for each repeated unit of forming fabric the velocity distribution pattern is obviously also repeatedly uniform. The smallest velocity occurs over the highest points of the fabric structure, the filaments' peak points; the maximum velocity occurs at the center points of the open areas. From knuckles to opens the velocity magnitude quickly but evenly becomes bigger and bigger. This repeatedly uniformity of velocity magnitude represents the fiber distribution in the dewatered fiber sheet is expected to be uniform too, which will afford good final paper product with light wire mark.

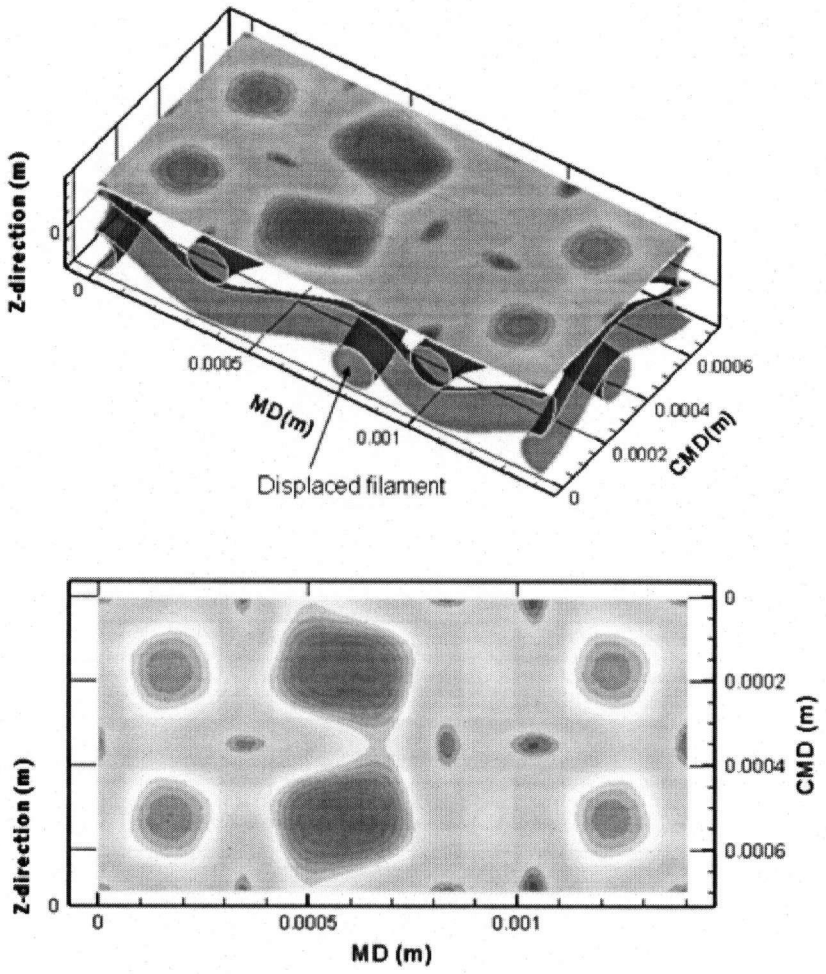

Figure 4.5: Isometric view and top view of the velocity magnitude contour at Plane 1, with 30% displaced filament, real space coordinate system.

Figure 4.5 and Figure 4.6 are the 3D velocity magnitude plots for a fabric structure with one filament displaced to its right side by 30% of

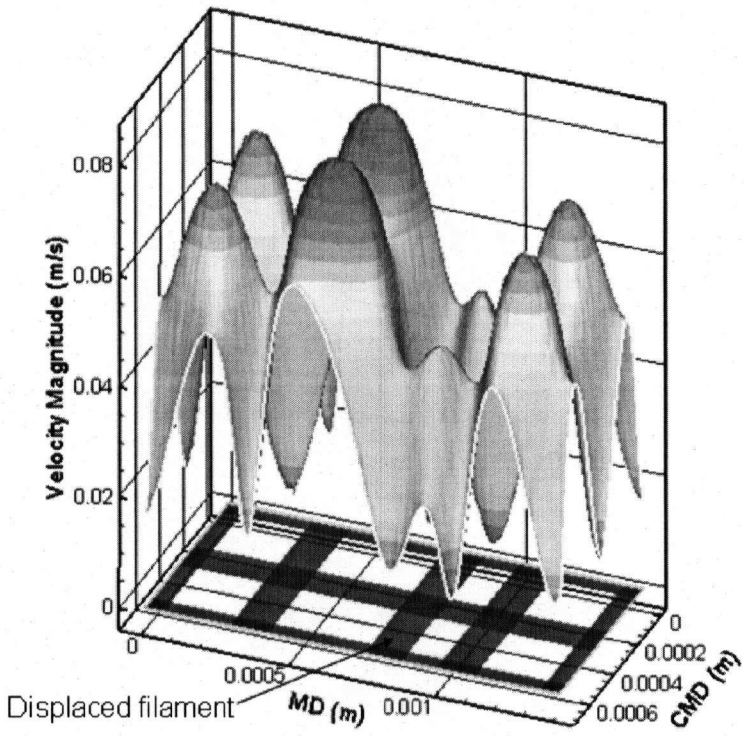

Figure 4.6: Isometric view of the velocity magnitude contour at Plane 1, with 30% displaced filament, Z-axis is the velocity magnitude in Plane 1.

the normal filament spacing. The location of the displaced filament is noted in the figures. For current fabric geometric structure, this is very close to the upper limit of the possible displacement in reality. In all other ways, the fabric is identical to that of Figure 4.3 and Figure 4.4.

From Figure 4.3 to Figure 4.6, a conclusion can be drawn that there is an obvious difference about the velocity magnitude distribution pattern between uniform case and non-uniform case. The case with uniform structure affords a uniform velocity distribution pattern, while the case with displaced filament results in a very uneven one and the mass flow rate between small pores and large pores is extremely different. The velocity magnitude around large pores is bigger than others, which means the fiber mass flow rate through that pore is higher. It represents more fiber will pass big pores and as a result, a fiber mat with uneven grammage will be formed. As discussed in Chapter 2, this sheet uneven grammage pattern will exist during pressing, drying and calendering processes, till the final stage of papermaking process, and become a major source of the heavy wire mark in paper product. Therefore, the displacement of the fabric filaments has a very adverse influence on the surface property of commercial paper sheets.

Figure 4.7 to Figure 4.12 illustrate the distribution of MD velocity component at Plane1. These plots maybe are a bit obscure for understanding. One clue can help them to be interpreted is that if the local MD velocity component is positive, the contour color for it will be warm color; if it is negative, then the contour color will be cold ones. For example, imagine that a CMD filament is split into two equal size halves by a CMD-Z direction plane passing the centerline of the filament, the pulp above the right half filament will have a velocity component in positive MD direction while passing that filament. Then at that spot the velocity contours will be colored by warm colors. The velocity magnitude around large pores is bigger than others, meanwhile the velocity vector map shown in Figure 4.11 illustrates that the velocity vectors tend to point toward large pores, too. Both of them are evidences of the non-uniform fiber distribution in fiber sheet. From these figures, the adverse effect of the displaced filament on the uniformity of the MD velocity component distribution can be clearly seen,

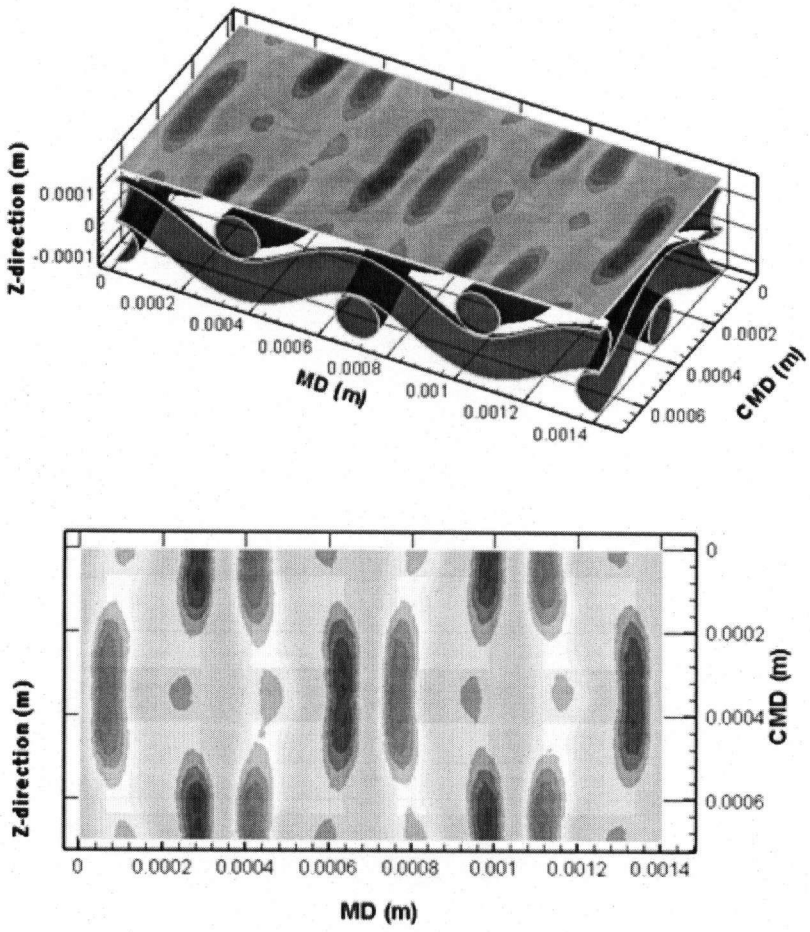

Figure 4.7: Isometric view and top view of the MD velocity component contour at Plane 1, uniform mesh case, real space coordinate system.

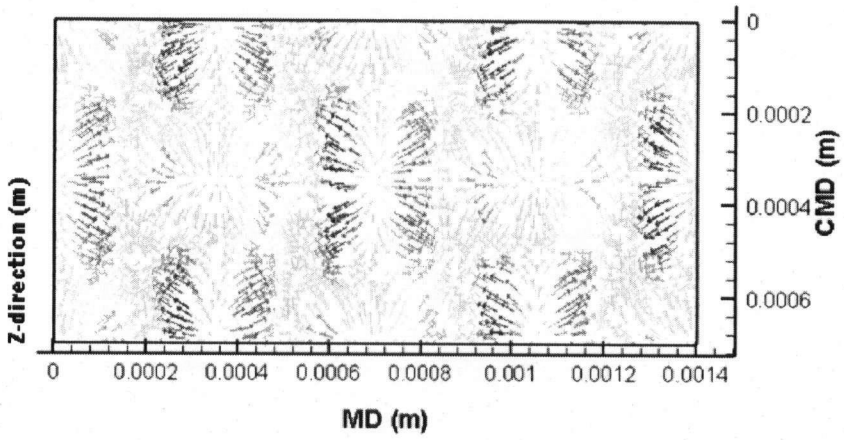

Figure 4.8: MD/CMD velocity vectors in Plane 1, uniform mesh case.

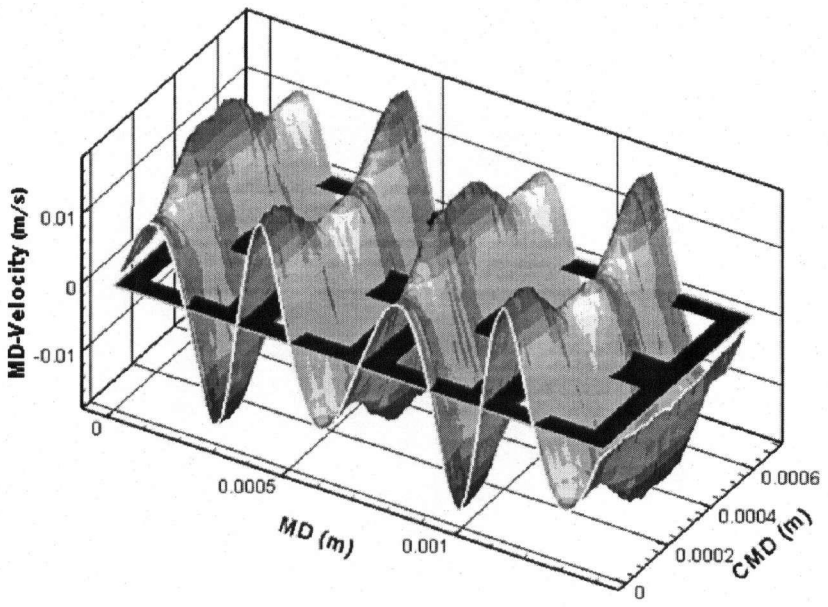

Figure 4.9: Isometric view of the MD velocity component contour at Plane 1, uniform mesh case, Z-axis is the MD velocity in Plane 1.

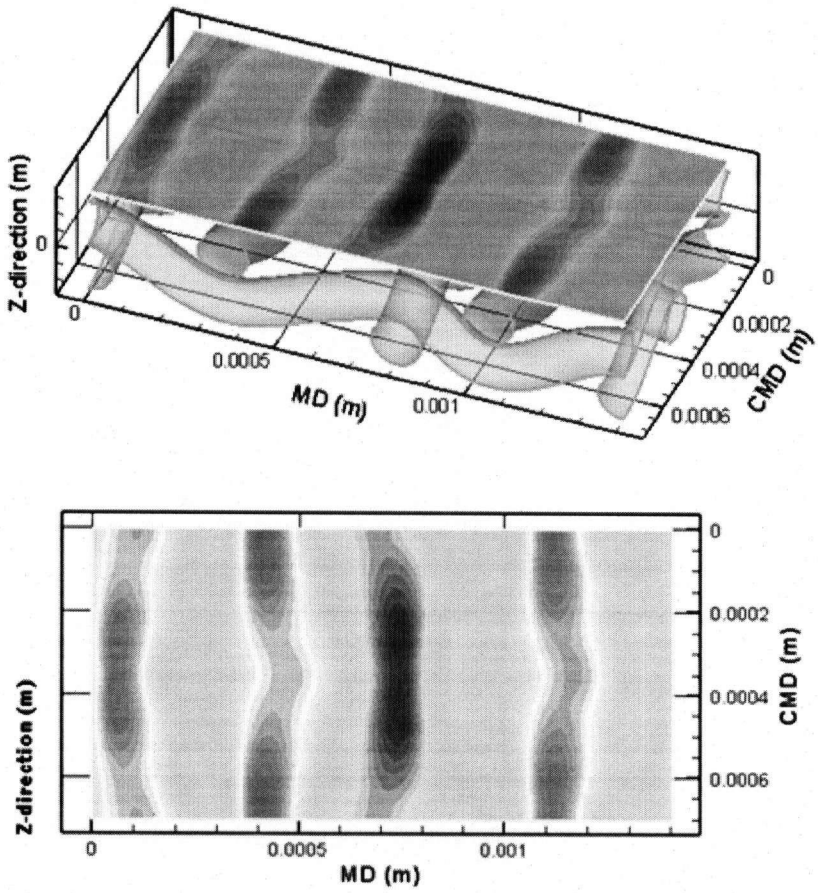

Figure 4.10: Isometric view and top view of the MD velocity component contour at Plane 1, with 30% displaced filament, real space coordinate system.

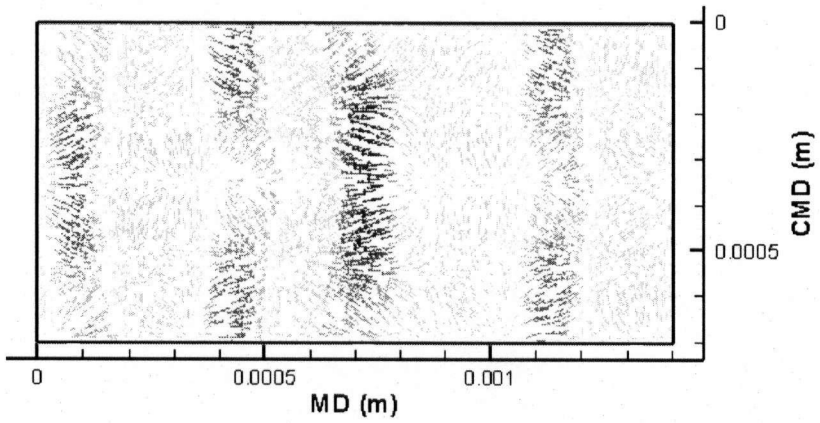

Figure 4.11: MD/CMD velocity vectors in Plane 1, with 30% displaced filament.

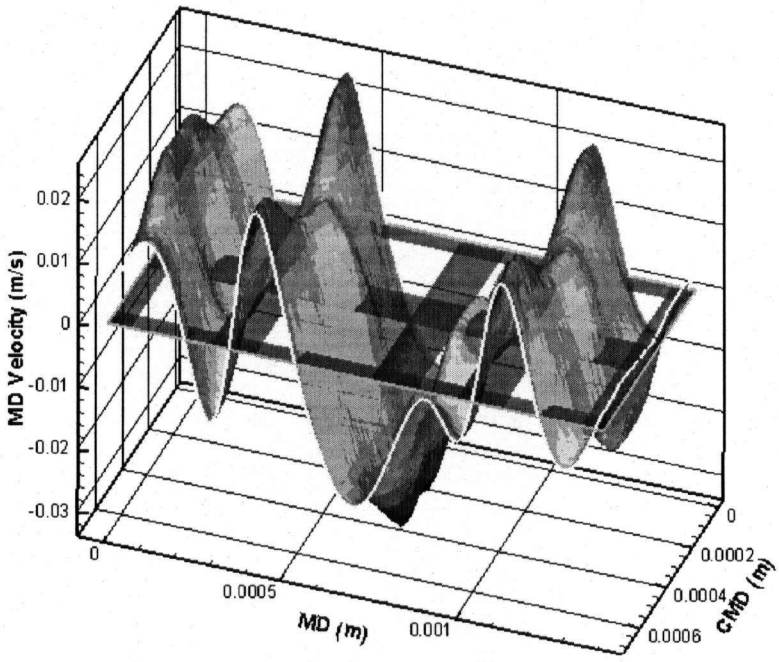

Figure 4.12: Isometric view of the MD velocity component contour at Plane 1, with 30% displaced filament, Z-axis is the MD velocity in Plane 1.

and this will radically do harm to the surface quality of paper sheet.

In the above 3D velocity study, only one filament was displaced. For cases where more than one filament is displaced, the major phenomena are highly similar with this case. To avoid redundancy, multi-filament displacement cases will be omitted here and will only be presented in 2D velocity plots.

4.1.3 Rake velocity results

Although plane velocity plots provide an intuitive viewing of the velocity distribution, they are somewhat unsuitable for quantitative analyses and comparison. Rake velocity plots are probably better for this purpose. As introduced in Section 4.1.1, the profiles are acquired from Rake 1 and Rake 2, two typical rakes extracted from Plane 1. Please see Figure 4.2 for reference. The vertical solid lines in the plots of this section represent the locations of the five CMD filaments' centerline in one repeated unit. The dash lines represent the locations of the displaced filament's centerline in non-uniform cases.

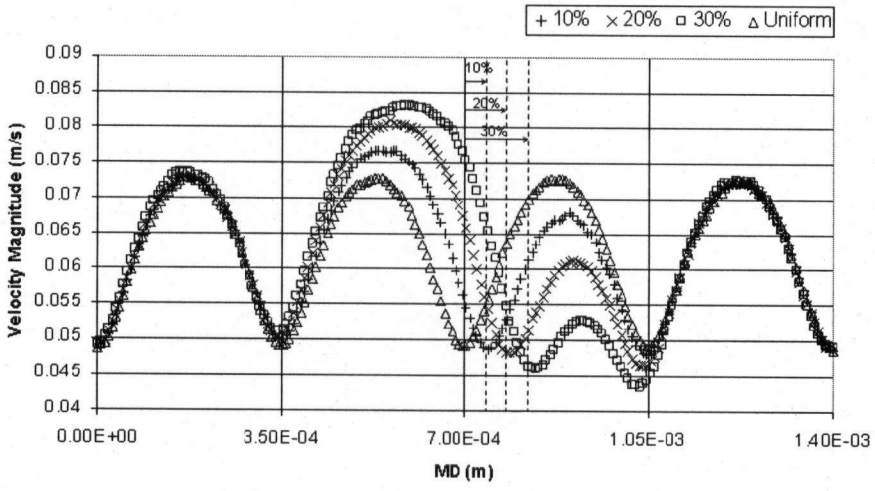

Figure 4.13: Velocity magnitude profiles along Rake 1 with different filament displacements.

Figure 4.13 and Figure 4.14 respectively illustrate the velocity magnitude profiles and MD velocity profiles of Rake1 for the different filament displacement cases. The selected displacements are 10%, 20% and 30%

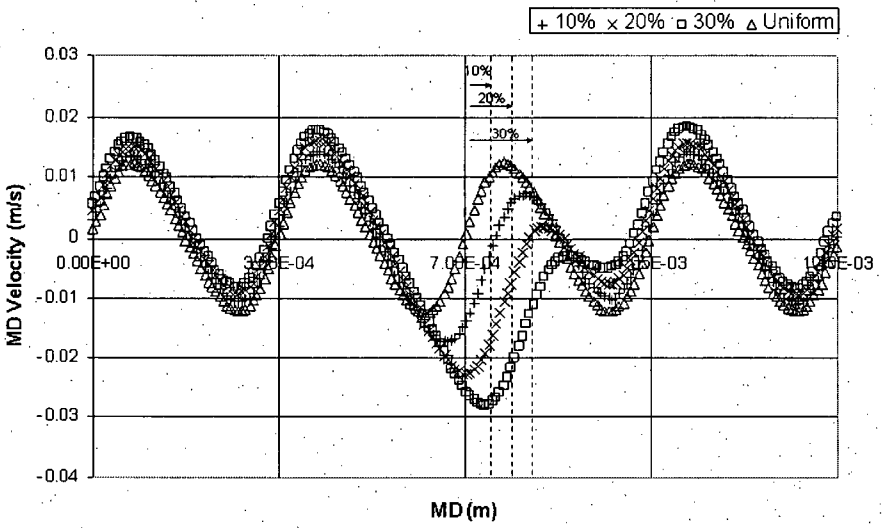

Figure 4.14: MD velocity profiles along Rake 1 with different filament displacements.

of the normal filaments spacing (L=0.35mm), which are enough for clearly presenting the trend of the velocity distribution.

It is clear that whereas in the uniform case the velocity profile is symmetric, with the increasing filament displacement the asymmetry of the velocity become more and more obvious. In the uniform case, the four local maximum values or peak values which occur in the centers of the four MD pores are the same. However, in the non-uniform cases the highest peak velocity magnitude occurs locally at the center of largest pore of the fabric while the lowest peak velocity occurs at the smallest one. In the 30% displacement case, the highest peak value will be 18% bigger than normal ones, and at the same time the lowest peak value will be 25% smaller than normal.

A more obvious trend can be seen in Figure 4.14. Because of the relatively smaller peak values for MD velocity component, the peak value (here refer to the local minimum value) difference even increases to 100% for the case with 30% filament's displacement. These differences in peak velocity will likely produce spatial anisotropy of fiber orientation and distribution, hence variations in local sheet grammage which will damage the paper surface quality.

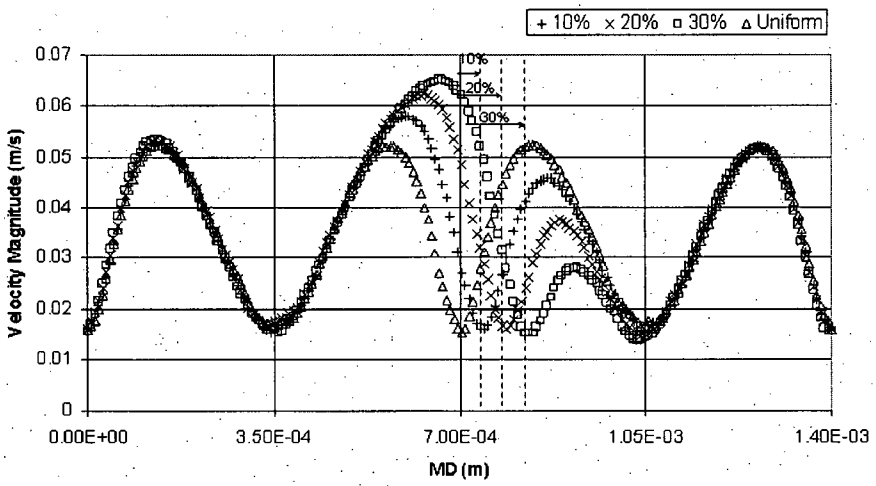

Figure 4.15: Velocity magnitude profiles along Rake 2 with different filament displacements.

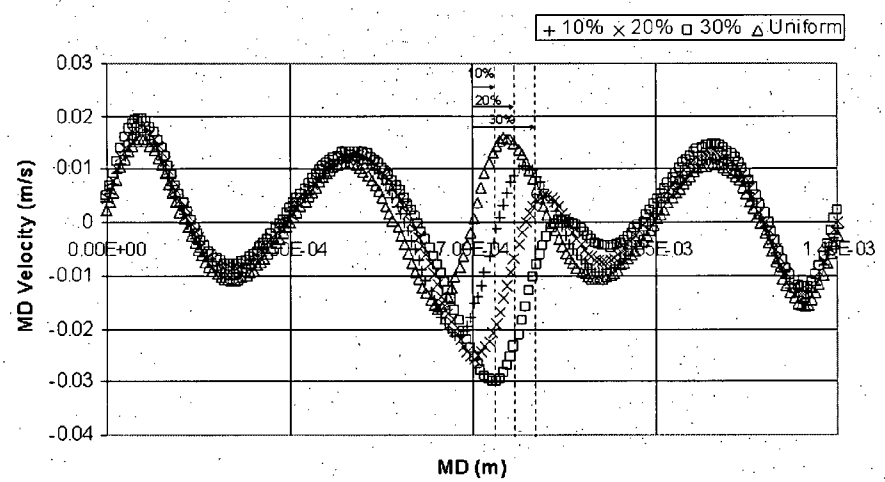

Figure 4.16: MD velocity profiles along Rake 2 with different filament displacements.

Figure 4.15 and Figure 4.16 show the velocity magnitude and MD velocity profiles of Rake 2. This rake is just above a MD filament and therefore the velocity magnitude and MD velocity is smaller than Rake 1. The same trends are apparent as with Rake 1: as the filament displacement increases, the non-uniformity of the velocity profile increases too.

Figure 4.17 and Figure 4.18 shows the velocity magnitude and MD velocity component profiles of Rake 1 when more than one filament is displaced relative to its initial location. Positive displacement means filaments move in the MD, negative value means filaments move in the opposite of the MD.

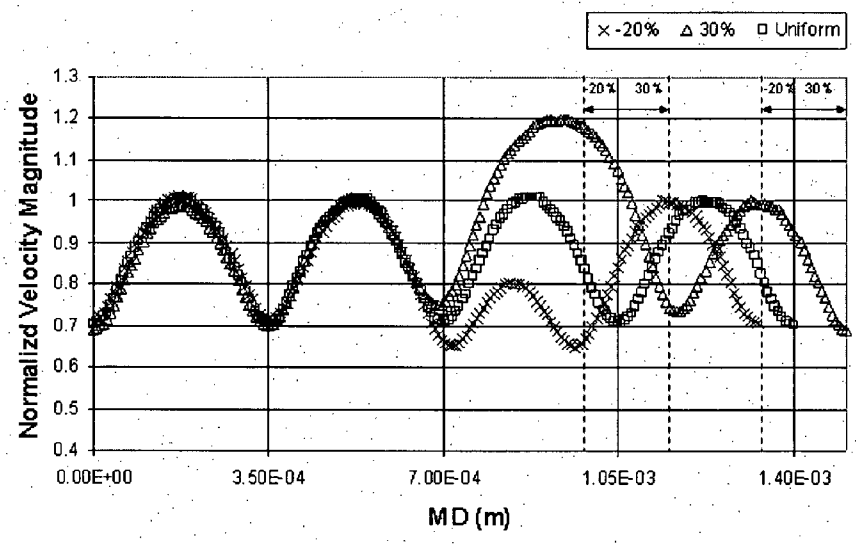

Figure 4.17: Effect of displacement of multiple filaments on velocity magnitude along Rake 1.

In this case, only one mesh pore along MD becomes larger and the other three remain the same size. Note that for this displaced case the velocity magnitude through all uniform pores is reduced relative to the uniform case, because of the imposed constant pressure drop boundary condition. After normalizing the local maximum/peak velocities of displaced cases by the peak velocity of uniform case, the velocity profiles are quantitatively comparable and the trend of profile variations is clear. In the case with filaments' 30% displacement, the normalized peak velocity magnitude of the larger pore is 20% higher than the nor-

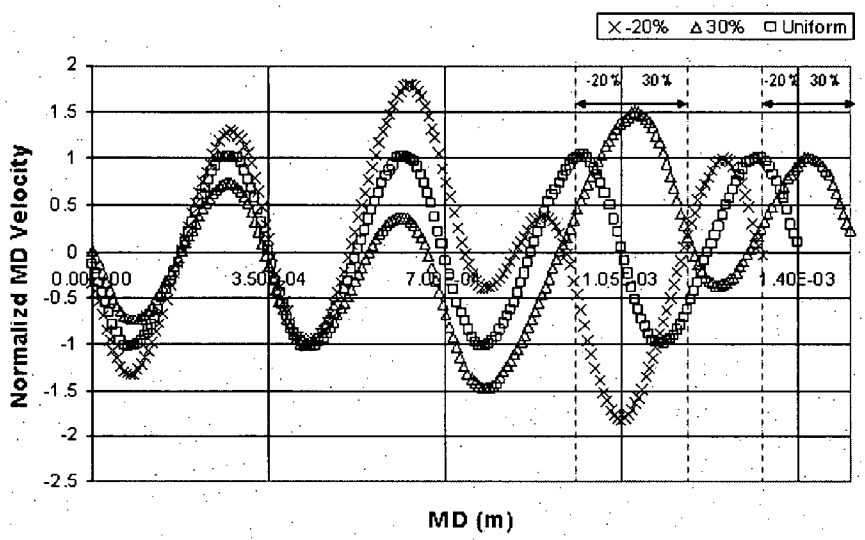

Figure 4.18: Effect of displacement of multiple filaments on MD velocity component along Rake 1.

mal ones; in the case with filaments' -20% displacement, the same value is 20% lower than normal. For MD velocity component, because of the velocity value is smaller, the trend is more obvious and the variation ranges change to 50% and -52% (lower), respectively.

Data from Rake 2 show similar trend. Figure 4.19 and Figure 4.20 illustrate the velocity profile results of Rake 2. The peak value variations for velocity magnitude respectively increase to 31% and -33% for the two displaced cases. This means the velocity fields above the MD filaments are more sensitive with the filaments displacement than the velocity fields over the pores.

In this section, the adverse effect of the filament's displacement on the velocity profile has been clearly illustrated. Next section, mass flow rate variation will be thoroughly analyzed.

4.2 Mass flow rate

In previous sections, it is known that the displacement of filament(s) will produce the variation of velocity distribution and result in the anisotropy of fiber orientation in fiber sheet. The mass flow rate through the fabric open areas is the other aspect that influences the

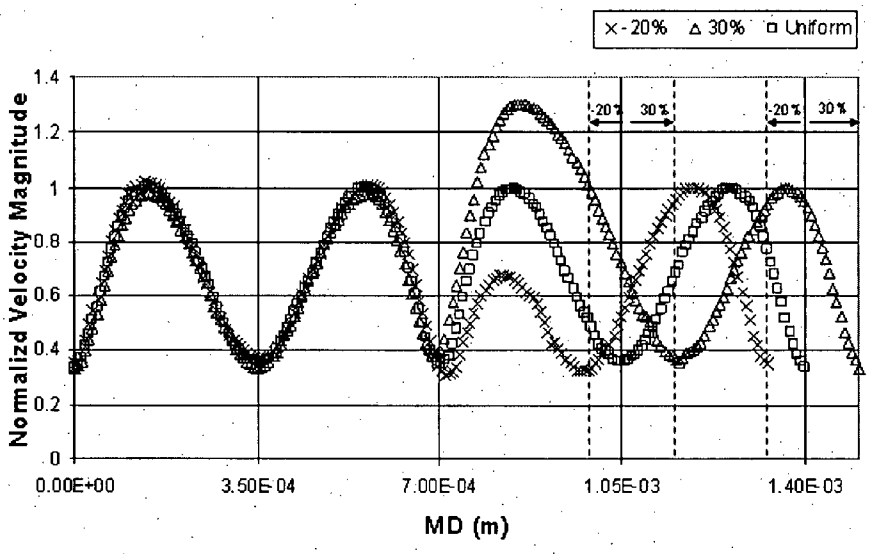

Figure 4.19: Effect of displacement of multiple filaments on velocity magnitude along Rake 2.

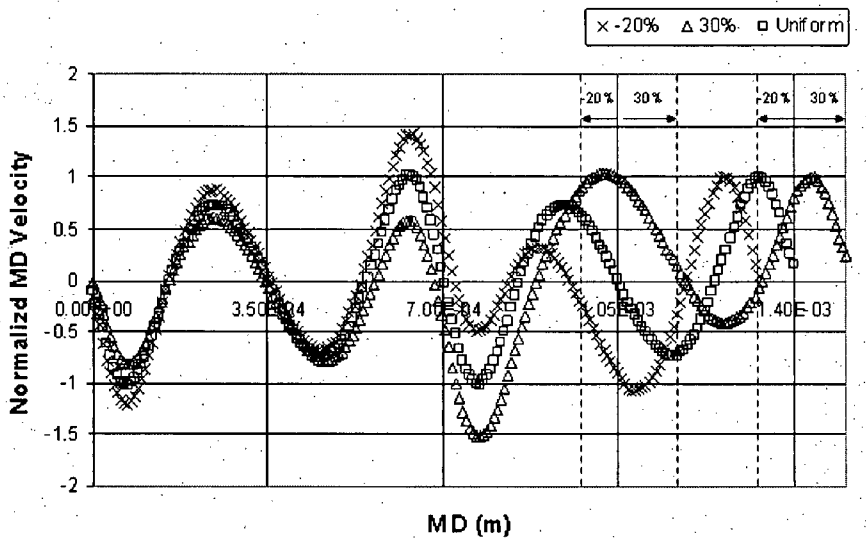

Figure 4.20: Effect of displacement of multiple filaments on MD velocity component along Rake 2.

fiber density distribution. Locations with a higher mass flow rate will have a heavier fiber sediment hence higher fiber density/grammage. This non-uniformity of the fiber density distribution will be apparent as wire mark or shadow mark on the surface of the paper.

4.2.1 Data acquisition

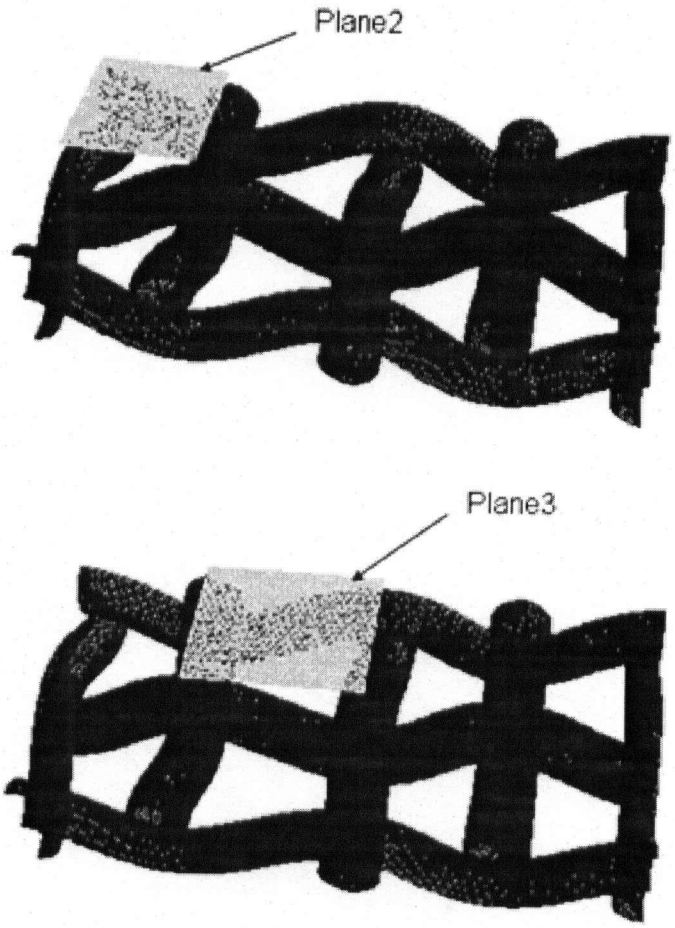

Figure 4.21: Isometric views showing the location of Plane 2 and Plane 3.

To measure the mass flow rate, two new auxiliary planes were set up in the flow field. Plane 2 is a cross-section perpendicular to the Z-direction, just over one of the normal pores of forming fabric; Plane 3 is a similar cross-section over the enlarged open. Refer to Figure 4.21 for their locations. Mass flow rates are surface integrate values of these planes.

4.2.2 Mass flow rate results

Table 4.1: Mass flow rate difference between normal pore and enlarged pore of forming fabric.

Displacement	Plane	Mass flow rate (kg/s)	Difference
30%	Plane 2	5.75E-06	57.80%
	Plane 3	9.08E-06	
20%	Plane 2	5.87E-06	38.40%
	Plane 3	8.12E-06	
10%	Plane 2	5.98E-06	19.00%
	Plane 3	7.12E-06	
Uniform	Plane 2	6.10E-06	0.10%
	Plane 3	6.11E-06	
-10%	Plane 2	6.22E-06	-19.10%
	Plane 3	5.09E-06	
-20%	Plane 2	6.34E-06	-36%
	Plane 3	4.07E-06	

Table 4.1 summarizes the mass flow rate numerical data of the 73*75 forming fabric. In this table, as has been illustrated in data acquisition section, the mass flow rate of Plane 2 and Plane 3 represent the mass flow rate of the normal pore and enlarged pore, respectively. All the differences of mass flow rate, which sever as the criterion of judging the density difference, are based on the mass flow rate of Plane 2. It is clear to see that with the increasing of the displacement, the mass flow difference and the non-uniformity of fiber density also increase.

Figure 4.22 is a plot of the results shown in Table 4.1 and more clearly shows the relation between fiber displacement and the variation of mass flow rate. The slope of the resulting plot is nearly 2. In other words, a 10% offset results in about a 20% difference in mass flow rate. The explanation for this magnification effect is that when the filament moves the area of the enlarged pore becomes bigger as does the average velocity of flow through that pore. From this point, a conclusion can be drawn that the filament displacement will strongly affect the fiber distribution and grammage of the paper sheet.

This mass flow rate results can be roughly validated by the pipe flow theory. See appendix B for details.

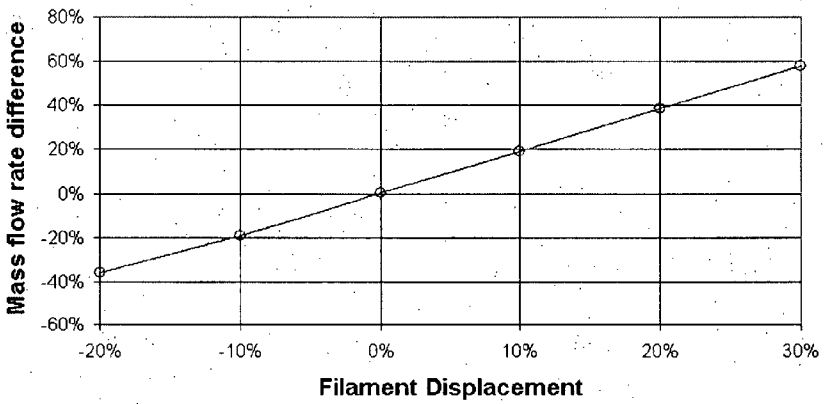

Figure 4.22: Difference between mass flow rate through enlarged area and through uniform areas, as a function of filament displacement.

4.3 Pressure drop

The pressure drop through wind tunnel screens and forming fabrics is often reported, so it will also be briefly discussed.

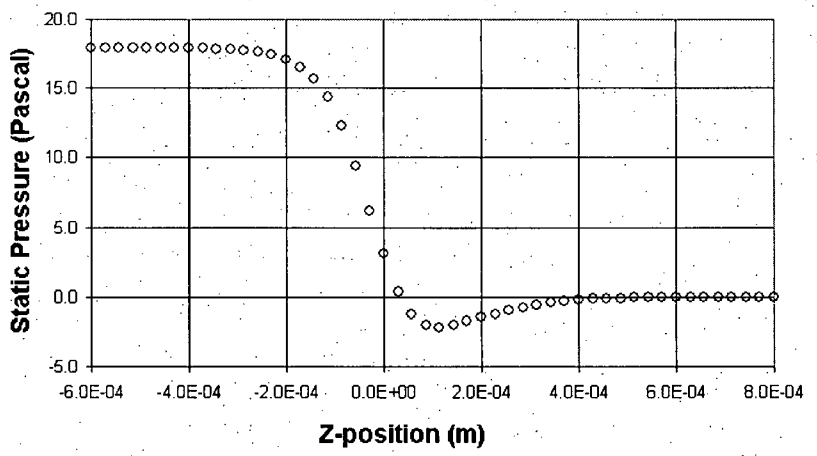

Figure 4.23: Pressure drop versus Z-position through forming fabric.

Figure 4.23 shows a typical pressure distribution along the Z-direction of a forming fabric. The forming fabric plane locates around the original point of Z-direction and normal to the Z-direction. After flowing through the fabric surface, the pressure decreases rapidly over a distance of approximately one filament diameter. This pressure decrease

is caused by the effect of drag on the individual filaments of the fabric.

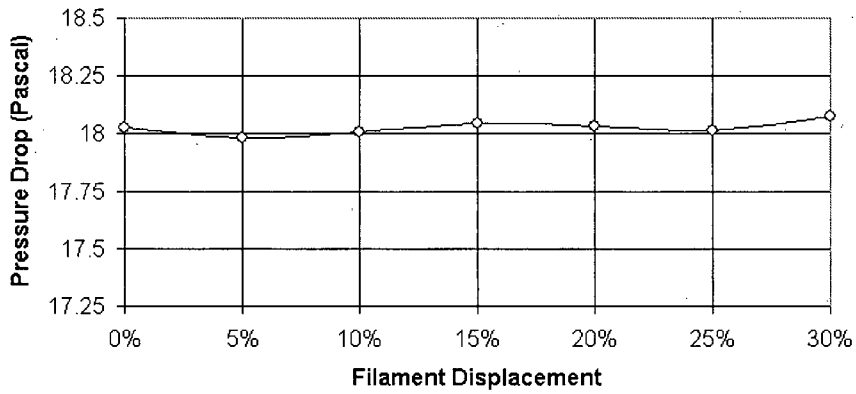

Figure 4.24: Pressure drop through forming fabric as a function of filament displacement.

Figure 4.24 shows that there is no obvious trend of pressure drop with filament displacement. The major reason is probably that, when considering the local filament displacement, the macroscopic open area ratio of the fabric screen remained constant. Thus, the filament surface area per unit flow area is also macroscopically constant. Assuming a nearly constant shearing stress on the fabric, the constant filament area implies a constant viscous drag and thus constant pressure drop. So, there is no relation between the pressure drop and the non-uniformity of the forming fabric. This analysis does not consider the effect of downstream vortex street on the viscous drag hence pressure loss, which may also has certain influence on this issue. The implication of this null result is that one cannot detect fabric non-uniformities of this sort by measuring the pressure drop through a fabric.

Chapter 5

Summary and Conclusions

5.1 Summary

In this research, a 3D numerical model of a square weave single layer forming fabric was developed to simulate the detailed dewatering process of forming section. The intent is to reveal the relation between the fabric's defective geometric structure and the upstream velocity/mass flow rate distribution, which will reflect the fiber distribution of the fiber mat formed on the forming fabric. This distribution will decide the uniformity of the fiber mat and then the wire mark characteristic of the final paper product. The ultimate goal is to understand the detailed dewatering mechanism of forming section in 3D level as well as provide a guide of forming fabric design and maintenance to obtain the best paper product.

The reliability of the geometric model, grid convergence, solver settings, and boundary conditions were checked. The experimental data of wind tunnel screen [4] was used to validate this numerical model since currently there is no 3D experimental data of forming fabric available. Accuracy analysis was done by GCI method recommended by I.Celik [40], a widely accepted method for CFD error estimation.

Then in the result illustration chapter, 3D velocity plots and 2D velocity profiles, both velocity magnitude and MD velocity, were presented. The velocity plots under imperfect geometric structure were compared with those of uniform case. Pressure drop and mass flow rate results under different cases were also discussed.

5.2 Conclusions

The three-dimensional flow through a simple square weave forming fabric has been simulated with CFD at low Reynolds numbers. Those simulations have shown:

- Good agreement between the simulation outcomes and experimental pressure drops through wind tunnel screens measured by other researchers has been found. This serves as a good validation for the numerical model applied in this study.
- The displacement of forming fabric filaments has a significant adverse influence on the uniformity of the upstream velocity distribution and mass flow rate through the different open areas of the fabric. The velocity anisotropy may result in anisotropy of the fiber orientation, while the mass flow rate discrepancy will produce variations in grammage in the dewatered fiber mat. Both of them will affect the surface quality, especially, the wire mark level of the final product. Therefore, the non-uniformity/displacement of the fabric filaments should be avoided.
- A 10% offset in the location of a filament produces approximately a 20% offset in the mass flow rate through that open area, relative to the uniform filament case. This magnification effect is result from when the filament moves the area of the enlarged pore becomes bigger as does the average velocity of flow through that pore.
- The pressure drop through a fabric is likely independent of the displacement of a single filament thereof. Therefore, it cannot be used to judge the fabric uniformity.
- Basing on GCI method, the accuracy of this numerical modeling is 3.0% for pressure and 1.9% for velocity.

Chapter 6

Suggestions for future work

Current work has established a simplified model of single layer forming fabric to investigate the relation between fabric geometric structure and velocity distribution, which has close relation with wire mark level of final paper product. Some fruitful results have already been achieved and shown in this thesis. However, further numerical and experimental works still need to be done to extend the understanding of the forming fabric dewatering process.

In the next stage of numerical study, a liquid-solid two-phase model for simulating the dewatering process could be built. The involvement of the fiber is expected to provide a more accurate prediction of wire mark level in the fiber mat. Efforts could be made to derive quantitative relations between fiber orientation and the geometric structure of the forming fabric. In this two-phase model, two models need to be developed and effectively combined together. One is used to describe the fluid motion in a three-dimensional domain with specific boundary conditions, as done in this research. Another model should describe fiber motion and orientation in the flow field. Since the fiber suspension is very dilute in the forming section, it can be simplified that the fibers will not alter the fluid pattern. So the above two models could be uncoupled in that the fiber state will not alter the governing equations for the flow. In other words, the two models may be solved consecutively.

Filtering process under high Reynolds number turbulent flow is another direction to be explored. Instead of using approximations, new model is closer to industry circumstances and prone to provide more reliable

and realistic results.

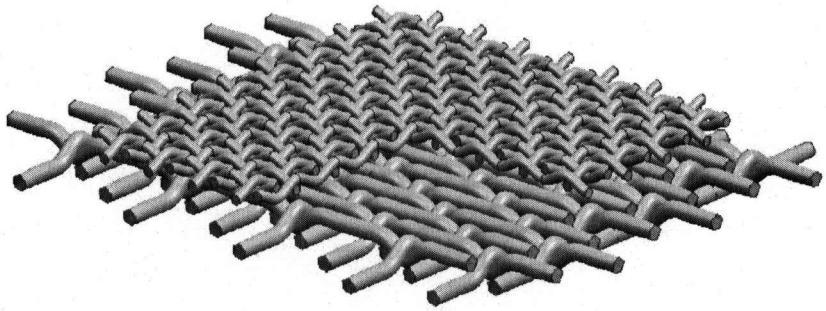

Figure 6.1: A typical 2/5 shed triple layer forming fabric(without binding yards).

The single-layer forming fabric with the simplest repeated geometry unit was studied in this thesis. Most forming fabrics applied in modern paper plant consist of multiple layers and have repeated patterns with greater complexity. For example, a 2/5-shed triple layer forming fabric has a repeated unit with 2*2 filaments in its top layer and 5*5 filaments in the bottom one. Refer to Figure 6.1. In future, more complex fabric model could be developed with the help of high-performance paralleled computer networks. Other geometric parameters, such as open area ratio, filament diameter ratio, filament spacing, and layer separation or offset could also be involved.

Three-dimensional experiments should also be done to test current and future numerical models and simulations. Some settings in current model, such as laminar fluid status, also need to be validated. Hydrogen bubble method for flow field visualization, dye injection technique and 3D PIV method are among the possible approaches.

Appendix A

Grid Convergence Independence(GCI) procedure

1. Decide the representative cell grid size h

Generally speaking, the wide applied definition of h is:

$$h = [\frac{1}{N}\sum_{i=1}^{N}(\Delta V_i)]^{\frac{1}{3}}, \tag{A.1}$$

Since the geometry is similar and the variables be interested in are the local/field ones, such as the pressure drop and the velocity distribution in front of the filaments, the grid size can be determined by the maximum grid volume:

$$h = [\Delta V_{max}]^{\frac{1}{3}}, \tag{A.2}$$

2. Decide the field variables

Two field variables were selected to be calculated the numerical accuracy. One is the pressure drop across the forming fabric, and the other is velocity distribution in front of the fabric filaments. Both of them are key variable of this study. It is desirable that the grid refinement factor

$$r = h_{coarse}/h_{fine}, \tag{A.3}$$

be greater than 1.3, which is base on experience.

3. Calculate the apparent order p

Use this equation set to solve the apparent order p iteratively:

$$p = \frac{1}{\ln(r_{21})} |\ln|\varepsilon_{32}/\varepsilon_{21}| + q(p)|$$
$$q(p) = \ln(\frac{r_{21}^p - s}{r_{32}^p - s})$$
$$s = 1sign(\varepsilon_{32}/\varepsilon_{21})$$

This equation set was solved by fixed-point iteration in Matlab.

After getting the apparent order, the accuracy for different variables can be achieved by some linear interpolations. See [40] for detail.

Appendix B

Mass flow rate validation

The mass flow rate data getting from the numerical simulation in Section 4.2 can be roughly validated by the pipe flow theory.

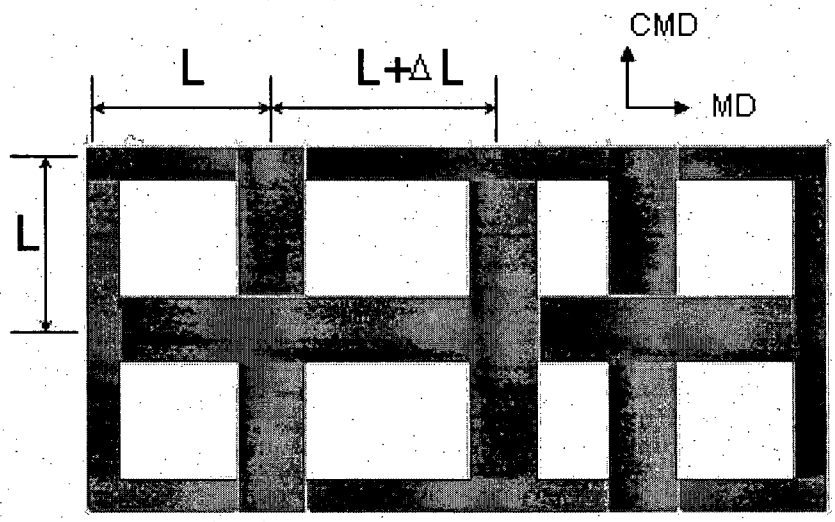

Figure 6.2: B.1: The geometric structure of the forming fabric with filament displacement.

The pores of the fabric can be treated as the cross-sections of very short pipes which are oriented along Z-direction, and the thickness of the fabric layer is then the length of the pipes.

The hydraulic diameter of the enlarged pore is given by:

$$D_h = \frac{2L(L+\Delta L)}{2L+\Delta L}, \qquad (B.1)$$

where

L = spacing between two parallel filaments
ΔL = filament displacement

Please refer to Figure B.1.

Then the pressure drop can be calculated from the pipe theory:

$$\Delta P = \frac{32V\mu l}{L^2}, \tag{B.2}$$

where

V = flow velocity
L = spacing between two parallel filaments
μ = viscosity coefficient of water
l = fabric thickness

Thus, the velocity and the mass flow rate of the normal pores or enlarged pores can be presented by a function of pressure drop, fabric thickness, and filament spacing. See Equation (B.3), Equation (B.4), and Equation (B.5):

$$V = \frac{\Delta P L^2}{32\mu l}, \tag{B.3}$$

$$Q = AV = \frac{\Delta P L^4}{32\mu l}, \tag{B.4}$$

$$Q_{offset} = \frac{L(L+\Delta L)\Delta P(2L^2+2L\Delta L)^2}{32(2L+\Delta L)^2\mu l}, \tag{B.5}$$

Figure B.2 shows the normalized mass flow rate values under different normalized offsets. The vertical coordinates is the mass flow rate normalized by the value of uniform case. The horizon coordinates is the offset normalized by the filament spacing. The spacing for nominal normalized offsets is the distance between the surfaces of two adjacent filaments, while the spacing for the real offsets is the distance between the centerline of them. From Figure B.2, it is clear that the numerical results are between two theoretical calculations, which means the former are highly credible.

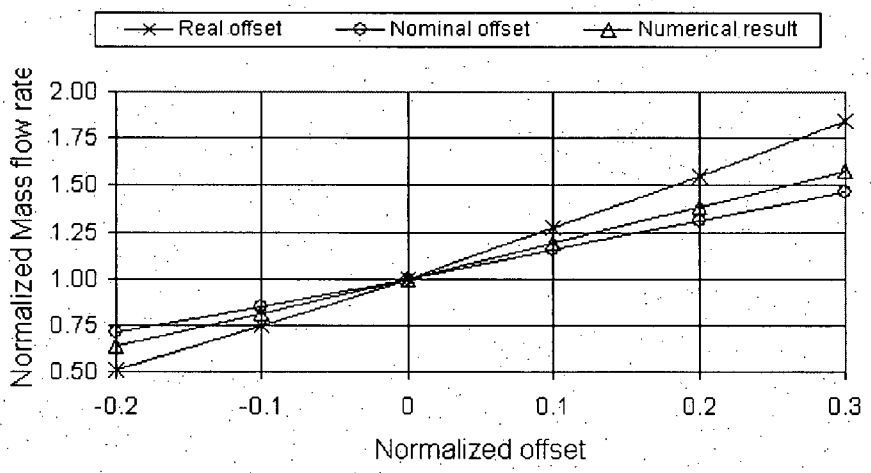

Figure 6.3: B.2: Normalized mass flow rates under difference normalized offsets.

Bibliography

[1] Hannu Paulapuro. *Papermaking Part 1, Stock Preparation and Wet End.* Fapet Oy, Helsinki, Finland, 2000.

[2] R.Danby. The impact of multilayer fabrics on sheet formation and wire mark. *Pulp and paper Canada*, 87(8):69–74, Aug. 1986.

[3] Zhaolin Huang. Numerical simulations of flow through paper machine forming fabrics. Master thesis, Mechanical Engineering Department, University of British Columbia, Vancouver BC Canada, 2003.

[4] G.B.Schubauer, W.G.Spangenberg, and P.S.Klebanoff. Aerodynamic characteristics of damping screens. *NACA*, Technical Note 2001, Washington, Jan. 1950.

[5] Cutler and H.Peter. Paper consumption patterns and growth. *Paper Technology*, 36(9):36–42, Nov. 1995.

[6] C.Earl Libby. *Pulp and paper science and technology, Volume2 paper.* McGraw-Hill, 1962.

[7] Josep Asuncion. *The Complete Book of Papermaking.* Lark Books, 2003.

[8] John R.Lavigne and Ken L.Patrick. *Pulp and paper dictionary.* Miler Freeman Books, 1993.

[9] Sam Herring and Tom Gulya. Engineered forming fabrics maximizes wear resistance; improve drainage. *Pulp and paper*, pages 91–93, Jan. 1995.

[10] J.H.Jong, W.D.Baines, and I.G.Currie. Experimental characteristics of forming fabrics and fiber mats. *Journal of pulp and paper science*, 25(3):95–99, Mar. 1999.

[11] Monica Shaw. Mills extract efficiency gains with modified forming, pressing fabrics. *Pulp and paper*, pages 49–54, Nov. 2004.

[12] Norman. On the mechanism of dewatering in the twin-wire and press sections. *Nordic pulp and paper research journal*, special issue:39–46, 1987.

[13] U.Aaltosalmi, M.kataja, A.Koponen, J.Timonen, A.Goel, G.Lee, and S.Ramaswamy. Numerical analysis of fluid flow through fibrous porous materials. *International paper physics conference*, pages 247–250, 2003.

[14] B.Heinola, R.Kilpelainen, J.Schlegel, and L.Maarve. The influence of forming fabrics on the retention and drainage on gap formers. *Pulp and Paper Canada*, 98(6):67–70, 1997.

[15] R.Danby. Impact of forming fabric structures on print quality. *Pulp and paper Canada*, 95(1):48–51, Jan. 1994.

[16] R.J.Kerekes, R.M.Soszynski, and P.A.Tam Doo. The flocculation of pulp fibers. *In transactions of the eighth fundamental research symposium, Ed. V.Punton. Mechanical Engineering Publications*, 1:265–310, Oxford, London, 1985.

[17] R.R. Farnood. Sensing and modelling of forming and formation of paper. Ph.D. thesis, Department of chemical engineering and applied chemistry, University of Toronto,Toronto ON Canada, 1995.

[18] M.K.Smith. Formation potential of west coast kraft pulps. *Pulp and paper Canada*, 87(10):69–76, Oct. 1986.

[19] E.S.Brazington and B.Radvan. A method of determining the substance over small areas of paper. *Tappi J.*, 42(7):545–548, 1959.

[20] O.Jokinen and K.Ebeling. Flocculation tendency of papermaking fibers. *Paperi ja Puu*, 67(5):317–325, 1985.

[21] J.Gorres, T.Cresson, and P.Luner. Sheet formation from flocculated structures. *JPPS*, 15(2):55–59, Jan. 1989.

[22] Pulp and paper Canada special report. Focus: high tech in paper machine clothing. *Pulp and Paper Canada, Westmount*, 103(2):17, Feb. 2002.

[23] R.Danby. The influcend of fabric strucutres on the two sides of sheets produced on twin-wire and hybrid formers. *Pulp and Paper Canada*, 90(2):41–48, Feb. 1989.

[24] R.Danby. Forming fabric design definition and selection: the means to machine and fabric efficiency. *Pulp and Paper Canada*, 101(8):36–41, Aug. 2000.

[25] R.Danby. P.plouffe print quality improvements through forming fabric design changes. *Pulp and Paper Canada*, 101(9):66–69, Sept. 2000.

[26] D.Chaplin. Image analysis: A powerful tool to pinpoint defects and gauge print quality. *CPPA Annual meeting*, Jan. 1997.

[27] R.Danby and H.Zhou. Numerical evaluation of the printability of paper surfaces. *Pulp and Paper Canada*, 105(9):38–42, Sept. 2004.

[28] H.Corte and O.Kallmes. Statistical geometry of a fibrous work. *Trans of the 2nd Fundamental research symposium, Francis Bolam, Ed. Techn. Sec. British Paper and Board Makers Assoc, Oxford, London*, pages 13–52, 1962.

[29] M.Deng and C.T.J.Dodson. Paper- an engineered stochastic structure. *Tappi press*, 1994.

[30] K.Niskanen, N.Nilen, E.Hellen, and M.Alava. Kcl-pakka: Simulation of the 3d structure of paper. *11th Fundamentals research symposium, Cambridge, Pira*, pages 1273–1291, Sept. 1997.

[31] C.Barratte, J.C.Roux, C.Voillot, and J.C.LeNest. Simulation of the formation of the 3d fibrous sheet: a new method. *51th annul conference ATIP.(Association of Paper Industry Technique),Grenoble*, pages 27–29, Oct. 1998.

[32] C.Barratte, J.C.Roux, C.Voillot, J.F.LeNest, J.C.Lonjon, and P.J.Mangin. Paper structure simulation: forming fabric input. *27th EU CEPA conference,Grenoble, France*, pages 125–131, Oct. 1999.

[33] R.Danby and A.Bouchard. Virtual reality sheet formation and printing (computer program). *TAGA*, pages 405–409, 1994.

[34] W.R.Givin and J.M.Hawes. Fiber retention and sheet formation modeling in fourdriniers and gap formers. *Appita*, pages 459–467, 1996.

[35] David McVey. Talking a closer look: Innovations in topographical analysis. *Pulp and paper Canada*, 106(10):12–15, Oct. 2005.

[36] S.I.Green. The twin wire former pressure distribution and the mechanism. http://batman.mech.ubc.ca/ green/PapermakingResearch.html.

[37] S.I.Green and R.Kerekes. Modeling the flow through a forming fabric. NSERC grant proposal, 2001.

[38] Chwan Pein Kyan. Flow of single-phase fluid through fibrous bed. Master thesis, Illinois Institute of Technology, USA, January, 1969.

[39] Xun Zhang. Fiber orientation in a headbox. Master thesis, Mechanical Engineering Department, Univesity of British Columbia, Vancouver BC Canada, 2001.

[40] I.Celik. Procedure for estimation and reporting of discretization error in cfd applications. Mechanical and Aerospace Engineering Department, West Virginia University, Morgantown, USA.

[41] Timothy Waung and S.Green. Summary of triple layer fabric simulations. Co-op projects, Mechanical Engineering Department, University of British Columbia, 2005.

[42] D.Johnson. Personal communictions. AstenJohnson Inc., 2002.

[43] Jan Wendler and Florian Schintke. Executing and observing cfd applications on the grid. *Future generation computer systems*, (21):11–18, 2005.

[44] Fluent Inc. Fluent 6.2 user's guide, vol. 3, chapter 24 using the solver. Lebanon, NH, 2005.

[45] J.P.Vandoormaal and G.D.Raithby. Enhancements of the simple method for predicting incompressible fluid flows. *Numerical Heat transfer*, 7:147–163, 1984.

[46] R.I.Issa. Solution of implicitly discretized fluid flow equations by operator splitting. *Journal of Computational Physics*, 62:40–65, 1986.

[47] J.H.Ferziger and M.Peric. *Computational Methods for Fluid Dynamics, Second Edition.* Springer, Berlin, New York, 1999.

[48] H.V.Patankar. *Numerical heat transfer and fluid flow.* Hemisphere, Washington D.C., 1980.

[49] M.M.Zdravkovich. Review of flow interference between two circular cylinders in various arrangements. *ASME Journal of Fluids Engineering*, 99:618–631, 1977.

[50] P.W.Bearman and A.J.Wadcock. The interaction between a pair of circular cylinders normal to a stream. *Journal of Fluid Mechanics*, 61(3):499–511, Mar 1973.

[51] P.G.Saffman and J.C.Schatzman. Stability of a vortex street of finite vortices. *Journal of Fluid Mechanics*, 117(4):171–185, Apr. 1982.

[52] X.N.Jiang, Z.Y.Zhou, J.Yao, Y.Li, and X.Y.Ye. Micro-fluid flow in microchannel. *International Conference on Solid-State Sensors and Actuators, Proceedings*, 2:317–320, 1995.

[53] P.J.Roache, K.N.Ghia, and F.M.White. Editorial policy statement on control of numerical accuracy. *ASME Journal of fluid engineering,*, 108(Mech issue), 1986.

[54] C.J.Fretias. Editorial policy statement on the control of numerical accuracy. *Journal of fluid engineering*, 115:339–340, 1993.

[55] L.F.Richardson. The approximate arithmetical solution by finite difference of physical problems involving differential equations, with an application to the stresses in a masonry dam. *Transactions of the royal society of London Ser.A*, 210:307–357, 1910.

[56] L.F. Richardson and J.A. Gaunt. The deferred approach to the limit. *Transactions of the royal society of London Ser.A*, 226:299–361.